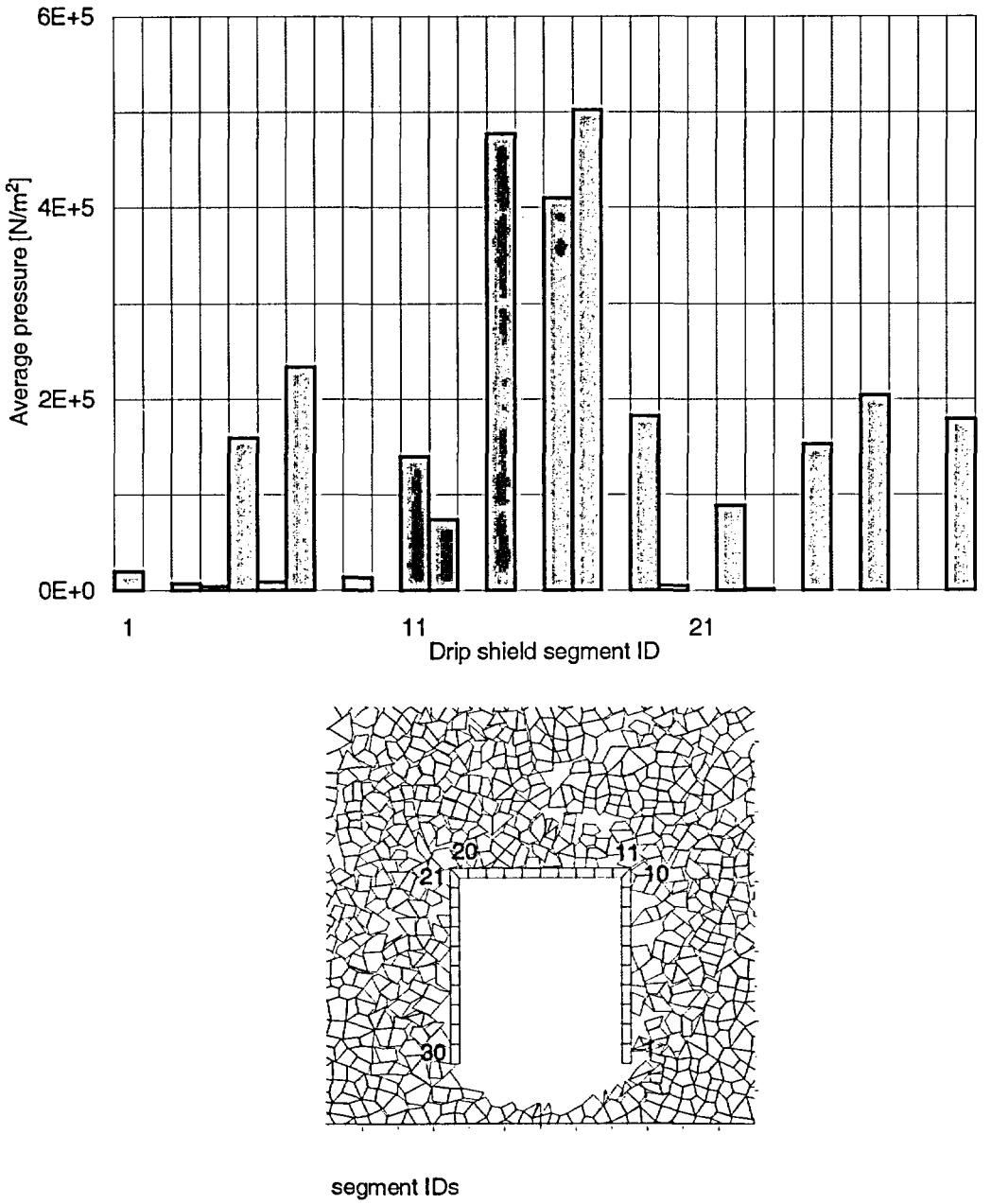

Figure 138. Pressures on the Drip Shield Calculated from the Discontinuum Model: Case 4

The evolution of rockfall and the cave size for case 4 as a function of strength degradation is shown in Figure 139. The model shows that in this case (lithophysal rock mass category 1 with unconfined compressive strength of 10 MPa), the emplacement drift is completely filled with caved rock after 80 percent degradation of the cohesive rock strength (Figure 139e). However, in the case of rock mass category 5, which has an unconfined compressive strength of 30 MPa (three times more than UCS for category 1), after 80 percent of strength degradation (Figure 139b), there will be some rockfall from the walls, but the drifts will, in general, be open.

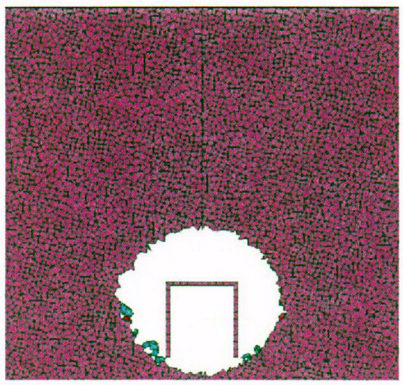

a) 100% cohesive strength

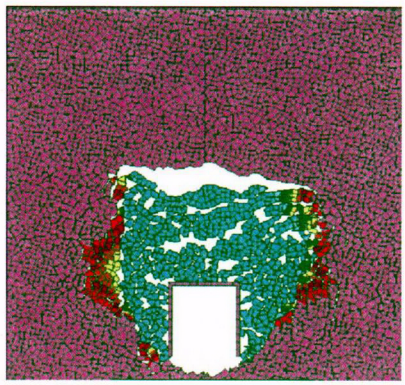

d) 40% cohesive strength

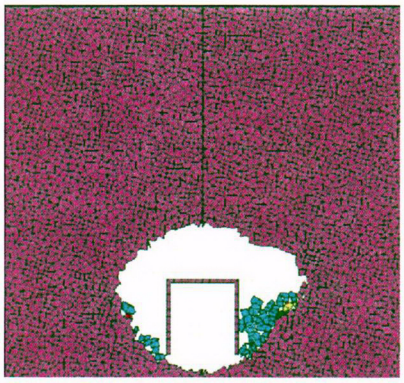

b) 80% cohesive strength

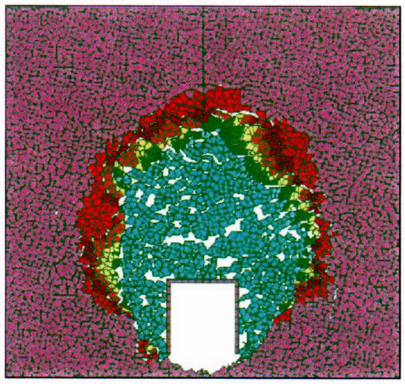

e) 20% cohesive strength

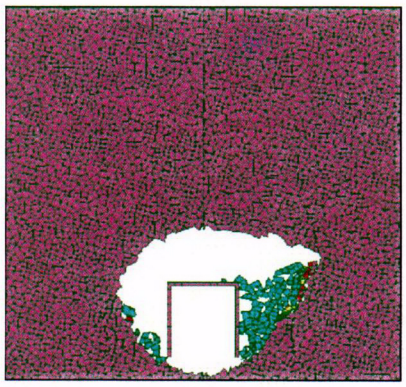

c) 60% cohesive strength

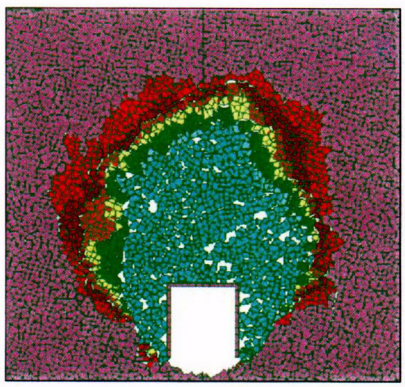

f) 0% cohesive strength

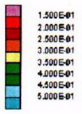

Displacement scale in m

Figure 139. Evolution of the Cave as a Function of the Cohesive Strength: Case 4

To demonstrate that selected block size of 0.2 m (cases 3, 4 and 5) does not effect the size or the shape of the predicted cave, the cave sizes are shown in Figure 140 for all three cases after complete strength degradation. There is certain level of randomness in the results, but the general trend is consistent. The results of average pressures on the drip shield from Table 40 also confirm that variability in the model results, as a function of the realization of the geometry of Voronoi blocks is relatively small.

Arching of stresses in case 4 around and inside the caved rock is shown in Figure 141.

6.4.2.5 Summary of Rock Mass Degradation in Lithophysal Units

The predictions of pressure of the caved rock on the drip shield by all three modeling approaches are summarized in Figure 142. As expected, analytical model yields the largest loads due to overly conservative conditions. The continuum numerical model accounts more accurately for transfer of load by friction from the caved rock to the surrounding stable rock mass. Consequently predicted loads for small bulking factors and large cavity size are much smaller than analytical predictions. When the bulking factor is large, the height of the cave becomes small. Stress arching cannot be realized within the small column of the cave rock and consequently, prediction between analytical and continuum models are identical. The most accurate approach, using the discontinuum model, does not use an imposed condition about the shape of the caved region. It also correctly accounts for load transfer through the caved rock. The predictions of the pressures on the drip shield using this approach are smaller than the predictions of the analytical and continuum models for all values of the bulking factor.

6.4.3 Investigation of Potential Key Blocks in Lithophysal Units

This section describes the probability of key-block existence, or the possibility that wedge-type failure occurs in the lithophysal units. The general approach used for analyses of wedge-type failure in the nonlithophysal units, as described in Section 6.3.1, is also applied in this study. The three-dimensional discontinuum code 3DEC is used for the mechanical analysis of the jointed rock mass simulated by FracMan. Since small-scale fractures have minor effect on wedge formation as confirmed in Section 6.3.3, only the fractures with trace lengths greater than or equal to 1 m long are included here.

Same as the nonlithophysal base case, a total of 76 fracture modeling regions were selected from the 100-m cube simulated FracMan jointed rock mass for Tptpll unit (Section 6.1). Since the coordinates of the 76 fracture modeling regions selected for the nonlithophysal units were randomly generated, they were also used in the lithophysal units. For conservatism and efficiency, joint strength parameters (cohesion and friction angle) were reduced to 0 to evaluate the probability of key-block existence. With strength parameter values assigned as 0, the predicted rockfall is equivalent to all blocks that are kinematically admissible to fall regardless of the frictional resistance of joint surface.

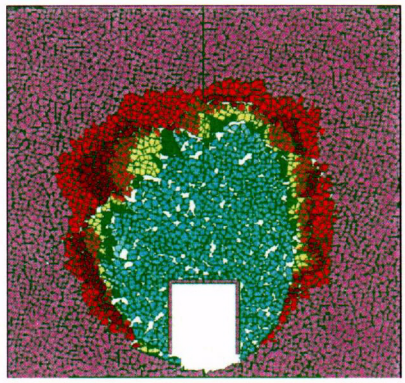

a) case 3

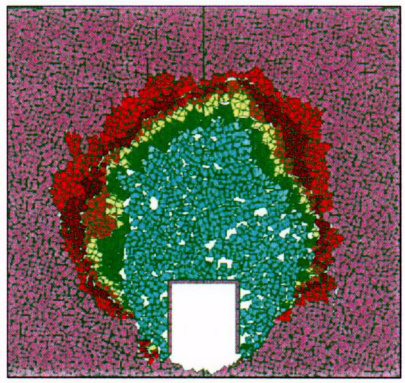

b) case 4

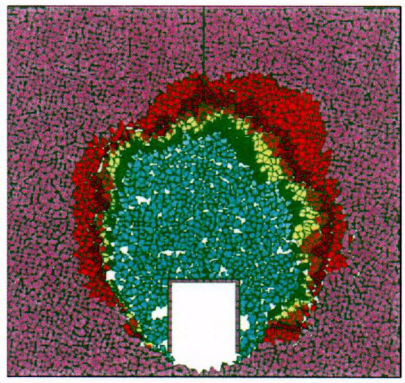

c) case 5

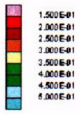

Displacement scale in m

Figure 140. Size and Shape of the Cave for Cases 3, 4, and 5

C62

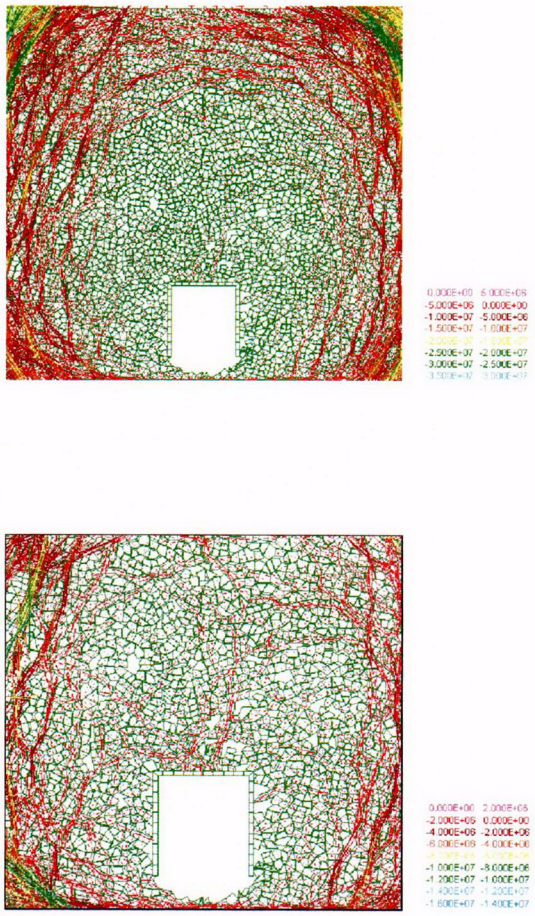

Stress scales in Pa

Figure 141. Stresses in the Rock Mass after Caving Shown at Two Scales

C63

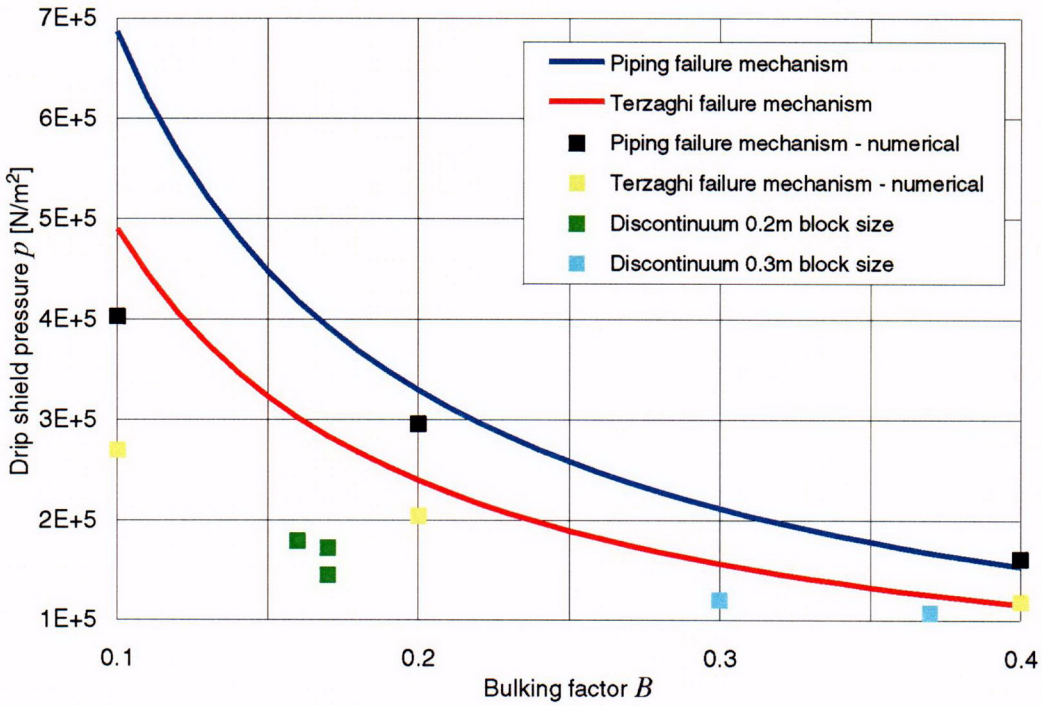

Figure 142. Summary of Vertical Load on the Drip Shield as a Function of Bulking Factor

The summary of the analyses is presented in Table 41. The distinct blocks existing in all simulations amount to only 24. Notice that the distinct blocks are the blocks that exist in the rock mass regardless of whether the blocks are kinematically or mechanically suitable to fall. A typical cross-section of the analysis with prediction of the distinct block is provided in Figure 143. Only two blocks were predicted to fall into the drift with a block volume of approximately 0.15 m^3 (0.36 tonnes) for both. With only two blocks predicted for almost 2 km of drift simulated while using extremely conservative (i.e., low) joint strength properties, the probability of key-block occurrence in lithophysal units is very low.

Table 41. Summary of 3DEC Rockfall Prediction for Lithophysal Units

Runs Completed	76
Number of Simulation Predict No Rockfall	74
Number of Simulation Predict No Distinct Block	61
Total Number of Rockfall	2
Total Volume of Rockfall (m^3)	0.31
Total Length of Drift Simulated(m)	1900
Number of Blocks per km	1
Volume of Rockfall per km (m^3/km)	0.16

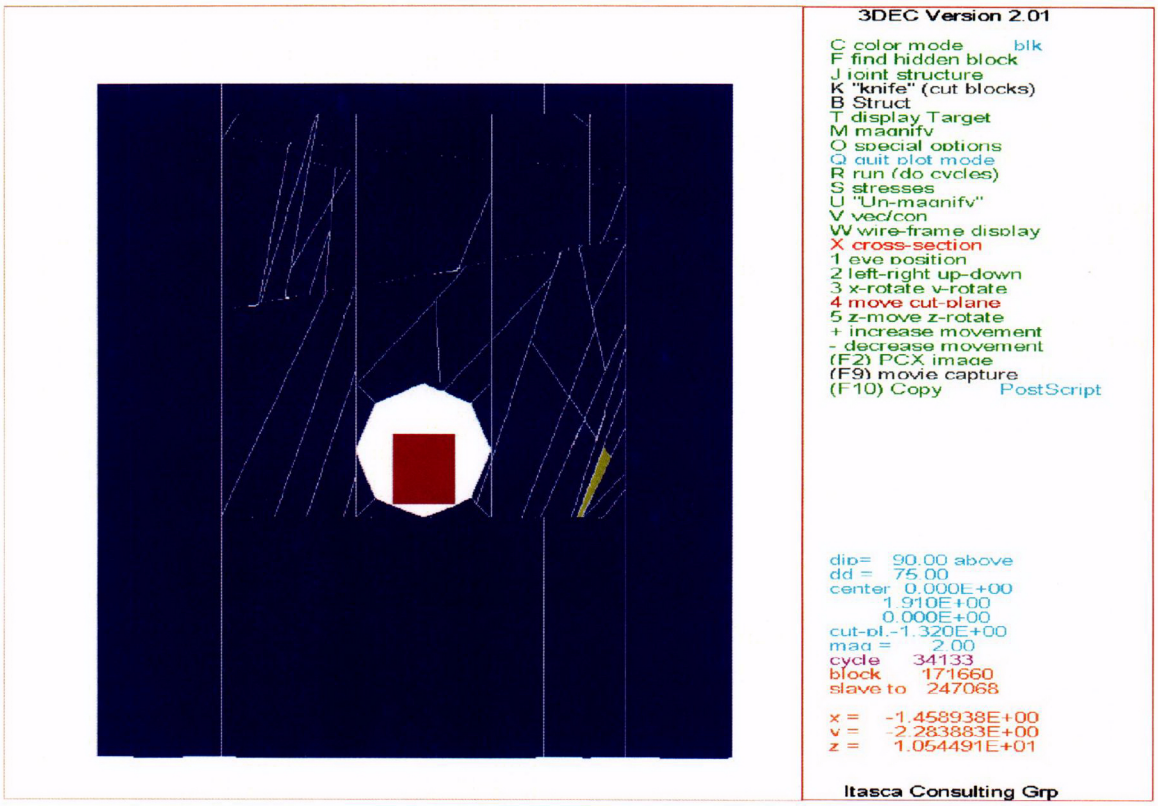

Figure 143. Cross-Section of a Typical Simulated Lithophysal Rock Mass in 3DEC

6.4.4 Drift Profile Prediction and Degraded Rock Mass Characteristics in Lithophysal Units

The distinct block approach applied in this analysis of lithophysal rock has provided a representation of the rock mass using an assembly of Voronoi blocks as described in Sections 6.4.1 and 7.7. This approach allows for internal fracturing to form and blocks to loosen and fail into the opening as the evolving stress states dictate. Progressive block failure continues until the crown becomes mechanically stable, and no additional blocks can fall. The final progressive failure surface provides the basis for the drift profile predictions presented in this section.

A depiction of worst-case profiles are provided, which are the outcome of UDEC analyses with the rock mass and opening subjected to in situ and seismic loadings. The worst-case drift profile resulting from preclosure ground motion is shown in Figure 110. The worst-case drift profile resulting from 1×10^{-6} postclosure ground motion is shown in Figure 115, which shows complete collapse of the drift opening. The 1×10^{-7} postclosure ground motion also results in complete drift collapse. For the preclosure period, thermally induced rockfall is in general minor due to ventilation.

Attachment XVIII includes the drift profiles for strength category 1 rock with consideration of seismic loading, thermal loading, and strength degradation. A total of 30 scenarios were provided. Attachment XVIII also provides information for degraded rock mass characteristics

C65

around the opening. The information consists of the stress tensor for UDEC zones, aperture change along the joints, and averaged volumetric strain.

6.5 UNCERTAINTIES AND LIMITATIONS

The task of predicting and characterizing drift degradation anticipated within repository emplacement drifts throughout the 10,000-year period of compliance for postclosure performance has several inherent uncertainties and limitations. These uncertainties are associated with both the modeling methods and the model inputs. To provide a meaningful assessment of drift degradation, the uncertainties must be identified and adequately represented within the model. The uncertainties associated with modeling methods are addressed with model validation (Section 7). Additionally, a discussion of alternative conceptual models has been provided (Section 6.7), which refutes plausible alternative models, thereby demonstrating that the drift degradation models presented in this report are adequate to account for all uncertainties and limitations.

This section provides a discussion of uncertainties associated with model inputs. The discussion below has been rank-ordered according to importance. That is, the parameters and their associated uncertainty that have the most significant impact on model results are discussed first.

Joint Geometry Data–The natural variability of joints within a rock mass represents epistemic uncertainty (i.e., uncertainty due to incomplete knowledge) in the design of structures in rock. The vast amount of joint data collected at the YMP provides a very good representation of the range of joints anticipated at the emplacement drift horizon. The range of joint geometry variability from tunnel mapping has been captured in the rockfall model for nonlithophysal rock through multiple simulations of the rock mass. Section 6.1.6 describes the generation of representative rock volumes using FracMan with the consideration of the natural variability of joints. The representativeness of the FracMan generated rock volume is validated in Section 7.8.2. Section 6.3.1.2.2 documents the random selection of the fracture modeling region in the rockfall analyses to cover the uncertainties associated with joint geometry data. The joint geometry is concluded to be the dominant factor for wedge-type rockfall in nonlithophysal rock. The uncertainty associated with joint geometry data in the rockfall models is assessed to be low.

Seismic Ground Motion Data–The seismic time histories used to evaluate rockfall reflect a number of variabilities, including epistemic uncertainty and randomness (aleatoric uncertainty). Epistemic uncertainties (due to incomplete knowledge) in the characterization of seismic sources and median ground motion attenuation, along with randomness in seismic ground motion, were explicitly incorporated into the probabilistic seismic hazard analysis. The mean results of that analysis form the basis for the site-specific ground motions used in this report. At annual probabilities of exceedance lower than about 1×10^{-6}, the mean hazard exceeds the 85th percentile of the hazard uncertainty distribution.

Development of site-specific ground motions incorporates additional epistemic uncertainty in the velocity and dynamic properties of site materials. Observed randomness of site materials is also addressed. Finally, randomness in the spectral content and duration of time histories that produce the same peak ground motion is accommodated in the drift degradation analyses through the use of 15 sets of time histories for each of the two postclosure hazard levels considered. The

earthquake magnitudes and epicentral distances of the recorded strong motion data that form an input to these time histories, reflect the range of magnitudes and distances contributing most strongly to seismic hazard at the site for the given annual probabilities of ground motion exceedance.

While the seismic ground motion inputs developed in this manner fully account for the underlying uncertainties and randomness, the result is that for annual exceedance probabilities of about 1×10^{-6} and lower, some realizations of ground motion are larger than the largest ground motions observed and may not be physically realizable. Nonetheless, these ground motions are consistent with and demonstrate fully the current state of uncertainty and randomness in deriving ground motion inputs for very low annual probabilities of exceedance. Currently lacking a technical basis to limit such ground motions to smaller values, these inputs are used in the analyses supporting TSPA-LA.

Intact Rock Physical and Mechanical Properties Data–A sufficient amount of intact rock physical and mechanical properties data has been collected for the nonlithophysal rock units. The epistemic uncertainty associated with this intact data for nonlithophysal rock is assessed to be low. Conversely, the amount of intact rock physical and mechanical properties data for the lithophysal units is limited. The epistemic uncertainty associated with this intact data for lithophysal rock is assessed to be high. To account for this uncertainty in the rockfall model for lithophysal rock, 6 categories of rock properties were included in the model to assess the impact of the ranges in intact properties data. The difference of rockfall prediction for the range of properties considered is provided in Section 6.4.

Joint Mechanical Properties Data–The amount of joint mechanical properties data for both the nonlithophysal and lithophysal rock units is limited; therefore, the uncertainty associated with this data is epistemic, and is relatively high. To account for this uncertainty in the rockfall models, sensitivity analyses for the possible range of joint strength parameters, dilation angle, and joint stiffness were conducted and the results are presented in Section 6.3.1.6. Joint mechanical properties appear to have secondary effect on rockfall comparing with joint geometry data.

Rock Mass Mechanical Properties Data–Rock mass mechanical properties data for nonlithophysal rock are calculated using rock mass classification data collected from field mapping within the ESF and intact rock properties data collected from laboratory testing. The uncertainties associated with the intact rock properties data are described above. The uncertainties associated with the rock mass classification data are epistemic, and are assessed to be low since an abundance of data has been collected based on established, industry-accepted methods. There is a moderate degree of epistemic uncertainty associated with calculation approach for assessing rock mass properties, since they are based on empirical methods and have an inherent characteristic of imprecision. This uncertainty has been accounted for by using two separate empirical calculation methods and demonstrating that the results are similar. The rock mass properties data are primarily used in the thermal-mechanical calculation to determine stresses within the model as described in Section 6.2, and is a relatively insensitive parameter to the stress calculations.

Rock mass mechanical properties data for lithophysal rock are based on large-diameter uniaxial compression test data and in situ slot test data (Attachment V, Section V.4.1). The epistemic uncertainty associated with this rock mass data for lithophysal rock is assessed to be high. To account for this uncertainty in the rockfall model for lithophysal rock, six categories of rock properties were included in the model to assess the impact of the ranges in rock mass properties data. The difference of rockfall prediction for the range of properties considered is provided in Section 6.4.

Rock Thermal Properties Data–A sufficient amount of rock thermal properties data has been collected for the nonlithophysal rock units. The epistemic uncertainty associated with this thermal properties data for nonlithophysal rock is assessed to be low. Conversely, the amount of rock thermal properties data for the lithophysal units is limited. Therefore, the epistemic uncertainty associated with this thermal properties data for lithophysal rock is assessed to be high. Uncertainty assessments are provided in the data source documentation identified in Table 2 and in Attachment V (Section V.5). Sensitivity calculations for thermal properties were conducted with one standard deviation less values used for thermal conductivity and specific heat as described in Section 6.2, Section 6.3.1.3, and Section 6.4.1.2. The sensitivity case results in approximately 23° higher peak temperature comparing with the base case but with minor impact to the rockfall prediction.

Repository Layout Information–The repository layout data is based on design information, which is currently in the preliminary design stage. This design information is subject to change before being finalized. The model results documented in this report are applicable for the emplacement drift diameter and emplacement drift alignment provided by repository design and performance assessment information exchange drawings (BSC 2002b; BSC 2003b; BSC 2003c) and Section 5.1.4 and 8.7 of *Underground Layout Configuration* (BSC 2002a). The rockfall models are sensitive to both emplacement drift diameter and alignment, and any change to this design information would require reevaluation.

6.6 DRIFT DEGRADATION FEATURES, EVENTS, AND PROCESSES

The development of a comprehensive list of features, events, and processes (FEPs) potentially relevant to postclosure performance of the repository is an ongoing, iterative process based on site-specific information, design, and regulations. The approach for developing an initial list of FEPs, in support of TSPA-SR (CRWMS M&O 2000b), was documented by Freeze et al. (2001). The initial FEP list contained 328 FEPs, of which 176 were included in TSPA-SR models (CRWMS M&O 2000b, Tables B-9 through B-17). To support TSPA-LA, the FEP list was re-evaluated in accordance with Section 3.2 of *The Enhanced Plan for Features, Events, and Processes (FEPs) at Yucca Mountain* (BSC 2002e). Table 42 provides a list of FEPs that are addressed in this model document, and provides specific references to sections within this document.

Table 42. FEPs Addressed by This Model Report

FEP No.	FEP Name	Section Where Disposition Is Described	Summary of Disposition in TSPA-LA
1.1.02.00.0B	Mechanical effects of excavation/ construction in EBS	6.1.4 V.4	A partial treatment of this FEP is provided in this report. The results of the rockfall models will be used in a separate analysis of EBS FEPs to determine the include/exclude status of the FEP for TSPA-LA. Specifically, this report provides rockfall models that are based on observation of rock characteristics representing the as-built (post-excavation) condition, so that potential excavation effects, if any, are considered. For example, the field mapping data of geologic features presented in Section 6.1.4 were collected post-excavation in the ESF, and therefore include excavation effects. Similarly, the calculation of rock mass properties in Attachment V (Section V.4) inherently includes these excavation effects. Therefore, the effects of excavation on rock mass response are reflected in the results presented in this report.
2.1.06.02.0A	Mechanical effects of rock reinforcement materials in EBS	5.5	A partial treatment of this FEP is provided in this report. The results of the rockfall models will be used in a separate analysis of EBS FEPs to determine the include/exclude status of the FEP for TSPA-LA. In this model report, no credit is taken for ground support in rockfall models (Section 5.3). Therefore, the consideration of the mechanical effects of rock reinforcement is implicit in the modeling approaches discussed in Sections 6.3 and 6.4. The rockfall models presented in this report (Sections 6.3 and 6.4) provide a bounding scenario in the analysis of the effects of rock reinforcement on drift degradation.
2.1.07.01.0A	Rockfall	6.3 6.4 7.8.4	A partial treatment of this FEP is provided in this report. The results of the rockfall models (i.e., block size distribution data for various seismic hazard levels) have been incorporated into consequence models for the seismic scenario for TSPA-LA to determine the include/exclude status of the FEP. Specifically, this report provides rockfall models that are based on site characterization data. Probabilistic descriptions of rock size and rockfall frequency are provided for use in engineering design analyses (Sections 6.3 and 6.4). The block size distributions and frequency of blocks presented in this report for static (i.e., no seismic) and preclosure ground motion are similar to the block size data developed using the approach in the previous version of this document (Section 7.8.4).
1.2.03.02.0B	Seismic-induced rockfall damages EBS components	6.3 6.4 7.8.4	A partial treatment of this FEP is provided in this report. The results of the rockfall models (i.e., block size distribution data for various seismic hazard levels) have been incorporated into consequence models for the seismic scenario for TSPA-LA to determine the include/exclude status of the FEP. Specifically, this report provides rockfall models that are based on site characterization data. Probabilistic descriptions of rock size and rockfall frequency are provided for use in engineering design analyses (Sections 6.3 and 6.4). The block size distributions presented in this report are similar to the block size distributions developed using the approach in the previous version of this document (Section 7.8.4). However, the frequency of blocks has increased with the larger ground motions used in this report compared to the previous approach (Section 7.8.4).

Table 42. FEPs Addressed by This Model Report (Continued)

FEP No.	FEP Name	Section Where Disposition is Described	Summary of Disposition in TSPA-LA
2.1.07.02.0A	Drift collapse	6.3 6.4 7.8.4	A partial treatment of this FEP is provided in this report. The results of the rockfall models (i.e., block size distribution data for various seismic hazard levels) have been incorporated into consequence models for the seismic scenario for TSPA-LA to determine the include/exclude status of the FEP. Also, drift profile results will be included into seepage abstraction models for TSPA-LA. Specifically, this report provides rockfall models that are based on site characterization data, including joint geometry and rock strength data, coupled with anticipated thermal stresses and seismic ground motion. Based on the analyses presented in this report (Section 6.3 and 6.4), minor degradation or collapse of drift is anticipated for the static (i.e., no seismic) case and during the preclosure period. The mechanical degradation or collapse of drift predicted for the static case and during the preclosure period is similar to the results from the previous approach using DRKBA (Section 7.8.4).
1.2.03.02.0A	Seismic ground motion damages EBS components	6.3 6.4	A partial treatment of this FEP is provided in this report. The results of the rockfall models (i.e., block size distribution data for various seismic hazard levels) have been incorporated into consequence models for the seismic scenario for TSPA-LA to determine the include/exclude status of the FEP. Specifically, this report provides rockfall models that are based on site characterization data, including joint geometry and rock strength data, coupled with anticipated thermal stresses and seismic ground motion. Based on the analyses presented in this report (Section 6.3 and 6.4), postclosure ground motion levels are sufficient to produce collapse of drifts in the lithophysal rock units (which represent approximately 75% of the emplacement drifts). Minor to moderate degradation or collapse of drift is anticipated in the nonlithophysal rock units throughout the regulatory period for postclosure performance.
2.1.11.07.0A	Thermal expansion/ stress of in-drift EBS components	6.2	A partial treatment of this FEP is provided in this report. The results of the rockfall models will be used in a separate analysis of EBS FEPs to determine the include/exclude status of the FEP for TSPA-LA. Specifically, this report provides rockfall models that include the potential impact of thermally induced stress changes in the rock mass (Section 6.2). The effects of thermally induced stress changes on drift degradation are documented in Sections 6.3.1.3 (nonlithophysal rock) and 6.4.1.2 (lithophysal rock).

6.7 DOCUMENTATION OF ALTERNATIVE CONCEPTUAL MODELS

Alternative conceptual models are based on assumptions and simplifications that are different from those employed in the base-case models (i.e., the rockfall model for nonlithophysal rock (Section 6.3) and the rockfall model for lithophysal rock (Section 6.4)). An important reason for considering alternative conceptual models is to help build confidence that changes in modeling assumptions or simplifications will not change conclusions regarding subsystem and total system performance. Conceptual model uncertainty results from sparse observational data and a lack of available information to corroborate or refute plausible alternative interpretations of the subsystem and the processes occurring within the subsystem.

The alternative conceptual models considered in this analysis of drift degradation are summarized in Table 43.

Table 43. Alternative Conceptual Models Considered

Alternative Conceptual Model	Key Assumptions	Screening Assessment and Basis
Continuum model of lithophysal rock	Lithophysae and fractures are smeared into the elements in the equivalent continuum representation of the rock mass. Rock damage is expressed as element yielding following the selected failure criterion.	The continuum model, such as FLAC or FLAC3D, is capable of modeling the material yielding behavior with elasto-plastic constitutive model. Yielding occurs when the stress state within the element reach the strength criterion specified by the constitutive law, the yielding of elements in the continuum, however, is not equivalent to rockfall. To estimate the extent of rockfall based on the depth of yielding could be too conservative. Therefore, this alternative conceptual model is excluded from further evaluation.
Continuum model of nonlithophysal rock	Fractures are smeared into the elements in the equivalent continuum representation of the rock mass. Element contains the weak plane information for potential shear slipping.	The compliant joint model (Chen 1987) is capable of analyzing jointed media behavior with fractures smeared into the elements. The model includes a continuum approximation based on average discontinuous displacements across joint planes within a representative elementary volume. The model also includes a material constitutive description based on linear elastic matrix material behavior and nonlinear normal and shear joint behavior between joint planes. The continuum model provides global rock mass response with predominant weak plane orientation, but can not predict wedge-type failure. Therefore, this alternative conceptual model is excluded from further evaluation.
Hudson and Priest (1979) model of nonlithophysal rock for estimating block size distribution	All joint planes are assumed to be perfectly planar, persistent, and extend throughout the rock volume of interest. The distribution of joint spacing values along a line are assumed to be of negative exponential form.	The approach to determine block size distribution using the Hudson and Priest approach has been documented by *Preliminary Block Size Calculation* (CRWMS M&O 1998b, Section 5.3). This approach provides a generalized statistical representation of the joint geometry. In particular, the assumption of continuous joints is not consistent with the discontinuous joints observed in the ESF. Since joint geometry is a primary factor in the assessment of block development, the generalized approach by Hudson and Priest does not provide the level of detail required to accurately model drift degradation. Therefore, this alternative conceptual model is excluded from further evaluation.

6.8 RESOLUTION OF KEY TECHNICAL ISSUES

The NRC is conducting an ongoing review of the information provided by the YMP activities to allow early identification and resolution of potential licensing issues. The NRC has identified several key technical issues (KTIs) and associated sub-issues, along with acceptance criteria for resolution of the issue. The drift degradation analysis provides information that is directly related to the KTI on Repository Design and Thermal-Mechanical Effects (NRC 2002). To provide a clear understanding of the technical issues, a NRC/DOE Technical Exchange and Management Meeting on Repository Design and Thermal-Mechanical Effects was held in February of 2001. As a result of this meeting, a number of agreements between the NRC and DOE were formally adopted (Reamer and Williams 2001), outlining the plan for resolution of the technical issues. The agreement items addressed in this report are presented verbatim as follows:

- **RDTME 3.04**–Provide in the Design Parameter Analysis Report (or some other document) site-specific properties of the host rock, as a minimum those included in the NRC handout, together with the spatial and temporal variations and uncertainties in such properties, as an update to the information contained in the March 1997 Yucca Mountain Site Geotechnical Report. The DOE will: (1) evaluate the adequacy of the currently available measured and derived data to support the potential repository licensing case and identify areas where available data may warrant additional field measurements or testing to reduce uncertainty. DOE will provide a design parameters analysis report (or other document) that will include the results of these evaluations, expected to be available to NRC in FY 2002; and (2) acquire data and/or perform additional analyses as necessary to respond to the needs identified in 1 above. The DOE will provide these results prior to any potential license application.

- **RDTME 3.05**–Provide the Rock Mass Classification Analysis (or some other document) including the technical basis for accounting for the effects of lithophysae. The DOE will provide a rock mass classification analysis (or other document), including the technical basis for accounting for the effects of lithophysae, expected to be available to NRC in FY 2002.

- **RDTME 3.10**–Provide technical basis for the assessment that two-dimensional modeling for emplacement drifts is considered to be adequate, considering the fact that neither the in-situ stress field nor the principle fracture orientation are parallel or perpendicular to emplacement drift orientation. The DOE will provide the technical bases for the modeling methods used in ground control analysis in a revision to the Ground Control for Emplacement Drifts for SR, ANL-EBS-GE-000002 (or other document) supporting any potential license application. This is expected to be available to NRC in FY 2003.

- **RDTME 3.15**–Provide field data and analysis of rock bridges between rock joints that are treated as cohesion in DRKBA modeling together with a technical basis for how a reduction in cohesion adequately accounts for thermal effects. The DOE will provide clarification of the approach and technical basis for how

reduction in cohesion adequately accounts for thermal effects, including any additional applicable supporting data and analyses. Additionally, the adequacy of the cohesion reduction approach will be verified according to the approach described in Subissue 3, Agreement 22 [RDTME 3.19], of the Repository Design and Thermal-Mechanical Effects Technical Exchange. This will be documented in a revision to the Drift Degradation Analysis, ANL-EBS-MD-000027, expected to be available to NRC in FY 2003.

- **RDTME 3.16**–Provide a technical basis for the DOE position that the method used to model joint planes as circular discs does not under-represent the smaller trace-length fractures. The DOE will analyze the available small trace-length fracture data from the Exploratory Studies Facility and Enhanced Characterization of the Repository Block, including their effect on block development. This will be documented in a revision to the Drift Degradation Analysis, ANL-EBS-MD-000027, expected to be available to NRC in FY 2003.

- **RDTME 3.17**–Provide the technical basis for effective maximum rock size including consideration of the effect of variation of the joint dip angle. The DOE will provide the technical basis for effective maximum rock size including consideration of the effect of variation of the joint dip angle. This will be documented in revisions to the Drift Degradation Analysis, ANL-EBS-MD-000027, and the Rockfall on Drip Shield, CAL-EBS-ME-000001, expected to be available to NRC in FY 2003.

- **RDTME 3.19**–The acceptability of the process models that determine whether rockfall can be screened out from performance assessment abstractions needs to be substantiated by the DOE by doing the following: (1) provide revised DRKBA analyses using appropriate range of strength properties for rock joints from the Design Analysis Parameters Report, accounting for their long-term degradation; (2) provide an analysis of block sizes based on the full distribution of joint trace length data from the Fracture Geometry Analysis Report for the Stratigraphic Units of the Repository Host Horizon, including small joints trace lengths; (3) verify the results of the revised DRKBA analyses using: (a) appropriate boundary conditions for thermal and seismic loading; (b) critical fracture patterns from the DRKBA Monte Carlo simulations (at least two patterns for each rock unit); (c) thermal and mechanical properties for rock blocks and joints from the Design Analysis Parameters Report; (d) long-term degradation of rock block and joint strength parameters; and (e) site-specific ground motion time histories appropriate for post-closure period; provide a detailed documentation of the analyses results; and (4) in view of the uncertainties related to the rockfall analyses and the importance of the outcome of the analyses to the performance of the repository, evaluate the impacts of rockfall in performance assessment calculations. DOE believes that the Drift Degradation Analysis is consistent with current understanding of the Yucca Mountain site and the level of detail of the design to date. As understanding of the site and the design evolve, DOE will: (1) provide revised DRKBA analyses using appropriate range of strength properties for rock joints from a design

parameters analysis report (or other document), accounting for their long-term degradation; (2) provide an analysis of block sizes based on the full distribution of joint trace length data from the Fracture Geometry Analysis for the Stratigraphic Units of the Repository Host Horizon, ANL-EBS-GE-000006, supplemented by available small joint trace length data; (3) verify the results of the revised DRKBA analyses using: (a) appropriate boundary conditions for thermal and seismic loading; (b) critical fracture patterns from the DRKBA Monte Carlo simulations (at least two patterns for each rock unit); (c) thermal and mechanical properties for rock blocks and joints from a design parameters analysis report (or other document); (d) long-term degradation of joint strength parameters; and (e) site-specific ground motion time histories appropriate for post-closure period. This will be documented in a revision to the Drift Degradation Analysis, ANL-EBS-MD-000027, expected to be available to NRC in FY 2003. Based on the results of the analyses above and subsequent drip shield calculation revisions, DOE will reconsider the screening decision for inclusion or exclusion of rockfall in performance assessment analysis. Any changes to screening decisions will be documented in analyses prior to any potential license application.

The contribution toward fulfillment of these agreement items provided by this model report is identified in Table 44.

Table 44. Repository Design and Thermal-Mechanical Effects Key Technical Issue Agreement Items Addressed in This Model Report

Agreement Item	Approach and Section Reference	Status of Agreement
RDTME 3.04	Geotechnical data to support the drift degradation analyses documented in this report are identified in Section 4, Section 7, and Attachment V. Discussions of data adequacy are provided throughout Sections 6, 7, and 8. Newly acquired data from lithophysal rocks have been used to develop the lithophysal rockfall model, including data from laboratory compression testing on large-diameter cores, and from in situ flatjack (slot) compression testing in the ESF main loop and ECRB Cross-Drift.	The data and information provided in this model report contributes to the closure of this agreement.
RDTME 3.05	The technical basis for accounting for the effects of lithophysae is presented in Section 6.4. The validity of this approach is discussed in Sections 7.3 and 7.4.	The data and information provided in this model report contributes to the closure of this agreement.
RDTME 3.10	The assessment of an appropriate approach to model the rock mass is a function of the specific repository host rock type: lithophysal or nonlithophysal rock (Section 7.1). For nonlithophysal rock, jointing controls the mechanical response, which is generally anisotropic in nature. Therefore, two-dimensional modeling of nonlithophysal rock is not realistic for rockfall modeling, and a three-dimensional modeling approach must be used. *Conversely, lithophysal rock is characterized by the presence of more-or-less uniformly distributed voids* (lithophysae) of varying size. Additionally, in the Tptpll, short trace length interlithophysae fracturing exists. Under these conditions, the representation of lithophysal rock as a homogeneous, isotropic rock mass is appropriate. Therefore, in models of drift stability, the use of a two-dimensional model in the plane perpendicular to the axis is adequate.	The data and information provided in this model report are intended to fully address the requirements of this agreement.
RDTME 3.15	Additional clarification of the approach and technical basis for how reduction in cohesion adequately accounts for thermal effects in the DRKBA analyses is provided in Attachment IV. However, the DRKBA analyses now provide a confirmatory role in the assessment of drift degradation. The drift degradation analyses are primarily conducted using UDEC and 3DEC, in which thermal loads have been explicitly modeled (Sections 6.3 and 6.4). The adequacy of the methods to account for thermal effects on drift degradation are validated in Section 7.8.	The data and information provided in this model report are intended to fully address the requirements of this agreement.
RDTME 3.16	The available small trace-length fracture data have been analyzed and included in this report, documenting their effect on block development (Section 6.3.3).	The data and information provided in this model report are intended to fully address the requirements of this agreement.
RDTME 3.17	The approach for determining the effective maximum rock size has been revised in this model report. The approach of varying the joint geometry input to UNWEDGE is no longer applied. The maximum rock size and shape is taken directly from the 3DEC output, which includes the variation in joint strike, dip, spacing, and persistence. The variation of joint geometry parameters is based on field mapping data from the ESF, which has been input into the rockfall model (Sections 6.1.6 and 6.3).	The data and information provided in this model report are intended to fully address the requirements of this agreement.

Table 44. Repository Design and Thermal-Mechanical Effects Key Technical Issue Agreement Items Addressed in This Model Report (Continued)

Agreement Item	Approach and Section Reference	Status of Agreement
RDTME 3.19	(1) In this revision of this model report, the DRKBA analyses provide a confirmatory role in the assessment of drift degradation. The primary analyses for degradation of nonlithophysal rock is provided using 3DEC (Section 6.3), while lithophysal rock is analyzed using UDEC (Section 6.4). An appropriate range of joint strength properties has been applied as documented in Section 6.3.1.6. Long-term degradation has been accounted for as documented in Section 6.3.1.5. (2) An analysis of block sizes based on the full distribution of joint trace length data has been included in this report (Sections 6.1.4 and 6.1.6), including the available small joint trace length data (Section 6.3.3). (3) As indicated above, the DRKBA results now provide a confirmatory role in the assessment of drift degradation. 3DEC has replaced DRKBA as the primary code for analyzing structural block development in the nonlithophysal rock units. The 3DEC and DRKBA results are in good agreement (Section 7.8.4). (a) Appropriate boundary conditions for thermal and seismic loading have been included in 3DEC as documented in Section 6.3.1.1. (b) A total of 76 fracture patterns have been analyzed, which were drawn from the same fracture population used in the DRKBA analyses (Section 6.3.1.1). (c) Thermal and mechanical properties for rock blocks and joints are available in the Technical Data Management System as documented in Section 4.1. (d) Long-term degradation of joint strength has been included as documented in Section 6.3.1.5. (e) Site-specific ground motion time histories appropriate for postclosure period have been modeled as documented in Section 6.3.1.2.	The data and information provided in this model report are intended to fully address the requirements of this agreement.

7. VALIDATION

7.1 INTRODUCTION

This section contains a discussion of the activities that were conducted to validate the mechanical material models and their implementation within qualified discontinuum numerical programs for mechanical representation of the repository host rocks. It is noted that the term "model" here refers first to the development and validation of the mechanical material models or representations for the two specific repository host rock types: lithophysal and nonlithophysal rocks. Secondly, validation refers to the examination of the implementation of these material models in a general numerical modeling scheme. In the case of the lithophysal rock, it is necessary to first discuss the existing laboratory database as a precursor to discussion of the implementation of this data in a numerical scheme. Validation of this implementation is addressed through comparison examples of the models to field and laboratory data.

The scope of the validation and the order of presentation are as follows:

- Lithophysal rocks
  - **Mechanical Material Behavior**–A discussion of the mechanical behavior of the lithophysal rocks is presented as the basis for development of the mechanical material model. The properties of this rock are controlled by the degree of lithophysal porosity as well as the interlithophysal fracturing. The lithophysae vary in size, shape, and in porosity vertically within the flow, but are distributed more-or-less uniformly locally within each unit. Since the diameter of the lithophysae are generally much less than the tunnel diameter, and, further, since they are uniformly distributed, a two-dimensional, isotropic equivalent mechanical material model can be used to describe their response to gravitational, thermal and seismic loading. The mechanical material properties of the upper (Tptpul) and lower (Tptpll) lithophysal units of the Topopah Spring formation have been determined from laboratory compression testing on large (11.5-in and 10.5-in diameter) cores, and from in situ flatjack (slot) compression testing in the ESF main loop and ECRB Cross-Drift.
  - **PFC (Particle Flow Code) Model Validation**–The purpose of the PFC program is primarily as a simulation tool for developing a detailed understanding of the effects of lithophysal porosity on rock mass behavior. The program is used to supplement limited field testing by providing a means for examining the effects of lithophysae variability on rock mass properties (i.e., as a supplement to laboratory and field testing). A mechanical material model for representing the elasticity and yield of these rocks is developed from the basic laboratory data using a "micromechanical" numerical model (i.e., PFC). The PFC model predictions are compared to laboratory measured rock properties as a means of validation.
  - **UDEC Model Validation**–Although the PFC program could theoretically be used to model tunnel-scale stability issues, the simulation times are too long for existing computer resources. Therefore, it is necessary to develop a simpler, engineering-based approach to represent the potential yielding and fracturing behavior of

lithophysal rock. This is done by creating an *equivalent* lithophysal mechanical model, which is implemented in the UDEC discontinuum program. The equivalent model is first calibrated such that it reproduces the basic laboratory mechanical response (as well as the PFC model response). The model is then validated via comparison to laboratory data, field observation of ECRB Cross-Drift tunnel mechanical response, and field thermal testing and brittle yield observed in the Drift Scale Thermal Test in the ESF. Additionally, a comparison of the UDEC program to a number of other dynamic jointed rock models for modeling of blast-related, lined tunnel stability conducted for the Defense Nuclear Agency is also given as a confidence-building exercise. These blasting simulations provide a difficult challenge for the models. The UDEC code itself is commercial software that is widely used internationally for design and research in rock engineering. The program has been extensively validated against analytic solutions and design problems that are documented in the User's Manual (Itasca 2002). This validation provides a comparison of UDEC to several discontinuum and continuum-based programs for solution of tunnels subjected to dynamic loading.

- Nonlithophysal rocks

  - **Geometric Fracture Modeling Using the FracMan Program**–The nonlithophysal rocks of the repository horizon include the middle and lower nonlithophysal units (Tptpmn and Tptpln, respectively). The rocks are typically fine-grained, strong and brittle extrusive volcanics whose mechanical behavior, under the stress conditions of interest, is governed by the network of non-persistent cooling fractures or joints. Since the jointing controls the mechanical response, the behavior is generally anisotropic in nature, requiring a three-dimensional analysis method. Development of a representative fracture geometry that adequately represents the variability of the actual rock mass is essential for representation of rockfall. Here, the FracMan program (see Section 3) is used for developing a "synthetic" fracture network based on the full periphery geologic maps and the detailed line survey measurements (CRWMS M&O 2000a; Mongano et al. 1999) conducted during tunnel boring operations in the ESF main loop and ECRB Cross-Drift. The synthetic fracture geometry is validated by comparing statistical analysis and full periphery maps of the synthetic and actual geologic maps.

  - **3DEC Model Validation**–The 3DEC discontinuum program is used to model the mechanical response of the fracture-rock block system in three dimensions. Fracture mechanical property data, in the form of shear strength and stiffness properties, are derived from rotary and direct shear test measurements as well as empirical correlations derived from underground mapping. Validation of the ability of the 3DEC program to represent this direct shear response for fractures as derived from laboratory direct shear testing of large cores is presented. Validation of the dynamic stability of a jointed rock mass through comparison of 3DEC to instrumented field tests is problematic. Specific, well-documented field examples of tunnels subjected to earthquake loading that would be suitable as validation examples were not identified. Therefore, the validation of the 3DEC program is performed through corroboration with an alternative numerical model (i.e., the key-block software,

DRKBA) to validate the 3DEC model results on block size distribution and rockfall frequency, and through use of an external technical review to validate the overall modeling approach. The 3DEC code itself is commercial software that has been used in international rock engineering practice for nearly 20 years. Validation of the 3DEC model for conducting static and dynamic mechanical simulations is first demonstrated by comparison of the model to analytic solutions and general engineering application in the code User's Manual (Itasca 2002).

7.2 MODEL VALIDATION LEVEL AND CRITERIA FOR VALIDATION

An analysis of the importance of the various process models used for input to the TSPA was assessed by performing sensitivity studies with the TSPA model. A discussion of the model calculations and conclusions is presented in *Risk Information to Support Prioritization of Performance Assessment Models* (BSC 2002f). The models discussed in this report do not supply information directly to the TSPA model. Instead, they supply input to the model describing the mechanical response of the drip shield which, in turn, interacts with the model of the mechanical performance of the waste package. Since the drip shield model is ranked as a Level I (described below), and, since the rockfall only impacts the drip shield performance, it is assumed that the rockfall modeling is also ranked as a Level I model.

The various process models were binned into one of three classes of importance to ultimate total system performance, or mean annual dose. These are: Level I, Level II, and Level III, with increasing level of importance of model to performance as the level increases. Models whose input property variation could lead to a potentially significant effect on the estimate of mean annual dose (e.g., a change greater than 1 mrem/year) should receive a high or Level III model validation. Models whose variation could lead to moderate effect on estimate of mean annual dose (less than 1 mrem/year but greater than 0.1 mrem/year) should receive Level II model validation. Level I validation is sufficient for models of less importance to the estimate of mean annual dose. According to the results of this study, the drip shield degradation model (for which this work is a direct feed) requires a Level I, or the lowest level of model validation. The Level I validation is described below.

7.2.1 Level I Validation

Level I validation should include, at a minimum, a discussion of documented decisions and activities that are implemented during the model development process that build confidence and verify that a reasonable, credible, technical approach using scientific and engineering principles was taken to:

A. Evaluate and select input parameters and/or data

B. Formulate defensible assumptions and simplifications

C. Ensure consistency with physical principles, such as conservation of mass, energy, and momentum

D. Represent important future state (aleatoric), parameter, and alternative model uncertainties

E. Ensure simulation conditions have been set up to span the range of intended use and avoid inconsistent outputs

F. Ensure that model predictions (performance parameters) adequately represents the range of possible outcomes consistent with important uncertainties.

Validation is to be performed using a single method as described in Section 5.4.1c of AP-SIII.10Q model validation procedure, consistent with a model of limited importance to the mean annual dose. Validation of drift degradation models is accomplished by the following methods:

- Corroboration with laboratory measurements or relevant observations not previously used to develop or calibrate the model
- Corroboration with results of alternative mathematical models developed independently
- Corroboration with data published in referred journals or literature
- Technical review by reviewers independent of the development, checking, and interdisciplinary review of the model documentation.

The TSPA-LA is relatively insensitive to the drift degradation models and therefore requires a low level of confidence. The appropriate level of confidence is achieved by demonstrating that the models conform to generally accepted physical principles.

The model validation activities discussed in this report follow the Level I validation requirements given in AP-SIII.10Q at a minimum, while exceeding these requirements in some instances. No further activities are needed to complete this model validation for its intended use.

7.2.2 Validation Criteria

The prediction of rockfall requires that the models be able to represent: (a) the geologic structure that creates rock blocks surrounding the tunnels, (b) the stresses induced by heating or ground motions, and (c) the interaction of the stresses and geologic structure, including the potential for intact rock mass failure, fracturing, and formation of rock blocks that can detach themselves from the surrounding rock mass. With these points in mind, the criteria for a Level I validation of the drift degradation models are as follows:

For mechanical models of nonlithophysal rock:

A. The geometry and variability of geologic structure needs to be represented in the FracMan (and 3DEC) model in a qualitatively reasonable fashion. Validation of the fracture geometries and their variability needs to be validated against field-measured geometry data from detailed line surveys and full periphery geologic maps. This validation is used to ensure that the resulting block geometries will reflect in situ block structure.

B. The mechanical constitutive model of the fractures in 3DEC needs to be validated against the laboratory direct shear testing data.

C. The ability of the numerical model to accurately represent seismic boundary conditions and wave transmission through the rock mass needs to be verified.

D. The overall ability of the model to adequately represent the dynamic stressing effects of the ground motion on rockfall needs to be validated.

For mechanical models of lithophysal rock:

A. The material model and analyses must account for the variability of rock mass properties resulting from variability of porosity in the lithophysal rock.

B. The material model and its numerical implementation must provide the ability to represent, in a realistic fashion, the yielding response of lithophysal rock in laboratory specimens and around tunnels, and the associated fracturing into blocks that can detach themselves from the surrounding rock.

C. The model must account for dynamic boundary conditions properly, and the subsequent interaction of dynamic stresses with rock mass yielding.

In addition to these specific, qualitative criteria, the model(s) (with the exception of the FracMan program) must be shown to properly implement the basic governing equations (in this case, the laws of motion) and to conserve energy. All of the numerical models discussed are commercially available software that have been extensively and rigorously tested. The programs have extensive User's Manuals that provide detailed derivation of the implementation of the governing equations, the mathematical description of the constitutive models, and verification of the accuracy and limitations of the programs through comparison of results to analytical solutions and example problems. These derivations and verification of ability to satisfy equilibrium and energy conservation are provided in the software User's Manuals (Itasca 2002).

The UDEC and 3DEC programs have been commercially marketed for approximately 20 years, and are used extensively in the civil construction, mining, waste disposal and geotechnical industries. The UDEC program, originally developed under contract to the U.S. Army Corps of Engineers, Waterways Experiment Station in the mid-1970's, was initially used as a publicly available research tool in geomechanics. The predecessor of UDEC, the Rigid Block Model, was developed in the early 1970's (Itasca 2002). Both UDEC and 3DEC have been used for design studies and analysis of field experiments on nuclear waste repository projects in the United States, Canada, Sweden, United Kingdom, France, and Finland. The PFC program has been available commercially for approximately eight years, although its initial development as a program for research in soil and granular materials mechanics dates to the late 1970's (Cundall and Strack 1979). Currently, PFC is being used extensively as a research and design tool in geomechanics, powder compaction, structural geology and tectonics, oil production, etc. A recent symposium dedicated to use of PFC (Konietzky 2003) provides a description of the extent of application of this approach.

7.3 MECHANICAL MATERIAL MODEL FOR LITHOPHYSAL ROCKS AND SELECTION OF INPUT PARAMETERS

7.3.1 Description of the Lithophysal Rocks

The Tptpul and Tptpll comprise roughly 85 percent of the repository emplacement area. A detailed description of the mineralogy, texture, fracturing and porosity are given in Section 6.1.4 and in Attachment XV. A review of the aspects of the geology important to the mechanical behavior is provided in this section. From a mechanical standpoint, the lithophysal rocks are composed of two distinct components: the matrix groundmass and the porosity. The matrix groundmass is, texturally and mineralogically, similar to the matrix of the nonlithophysal rocks. The primary difference in the groundmass of the Tptpll and Tptpul is in the extent of fractures. The Tptpll is intensely fractured with short-length, inter-lithophysal fractures, which have a predominant vertical orientation with spacing on the order of inches. Figure 144a is a photograph of a 12-in. diameter core sample removed from the Tptpll showing the intensely fractured nature of this unit, creating intact block sizes a few inches on a side. This is contrasted by Figure 144b showing the wall of an alcove in the Tptpul, off the ECRB Cross-Drift, showing the typical unfractured matrix groundmass in this unit.

The rock mass porosity in the lithophysal units has been shown to be the primary physical factor that governs elastic and strength properties (Price et al. 1985). The porosity is found in three basic components: the matrix grain to grain porosity, which averages around 10 percent in all of the Topopah Spring sub-units (Price et al. 1985); the lithophysal void porosity; and the porosity of alteration which includes lithophysal rims and spots. Figure 145 shows the variation in lithophysal cavity percentage within the Tptpll in the ECRB Cross-Drift as determined by direct tape and angular measurement (Attachment XV). This plot shows that the lithophysal cavity porosity varies from approximately 10 to 30 percent with variability on a scale of 5 to 10 m.

The lithophysal cavities vary in size and shape, with characteristics that are somewhat different in the Tptpul and Tptpll. The lithophysae in the Tptpul:

- Tend to be smaller (roughly 1 to 10 cm in diameter)
- Are more uniform in size and distribution within the unit
- Vary in infilling and rim thicknesses
- Have a volume percentage that varies consistently with stratigraphic position
- Are stratigraphically predictable.

In contrast, the lithophysae in the Tptpll:

- Tend to be highly variable in size, from roughly 1 cm to 1.8 m in size
- Have shapes that are highly variable from smooth and spherical to irregular and sharp boundaries
- Have infilling and rim thickness that vary widely with vertical and horizontal spacing
- Have volume percentages that vary consistently with stratigraphic position
- Are stratigraphically predictable.

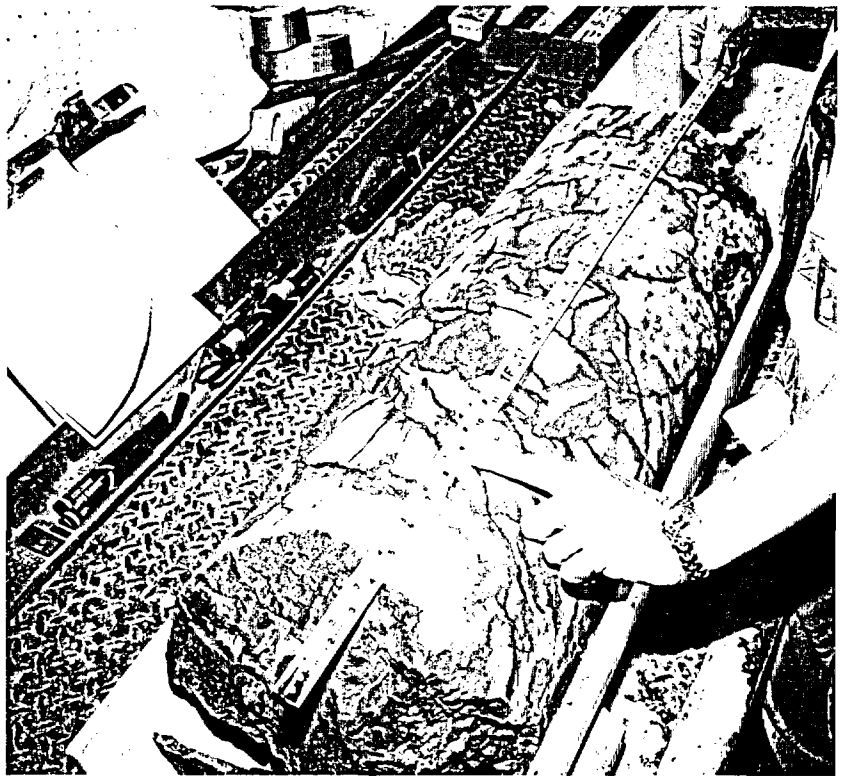

a)

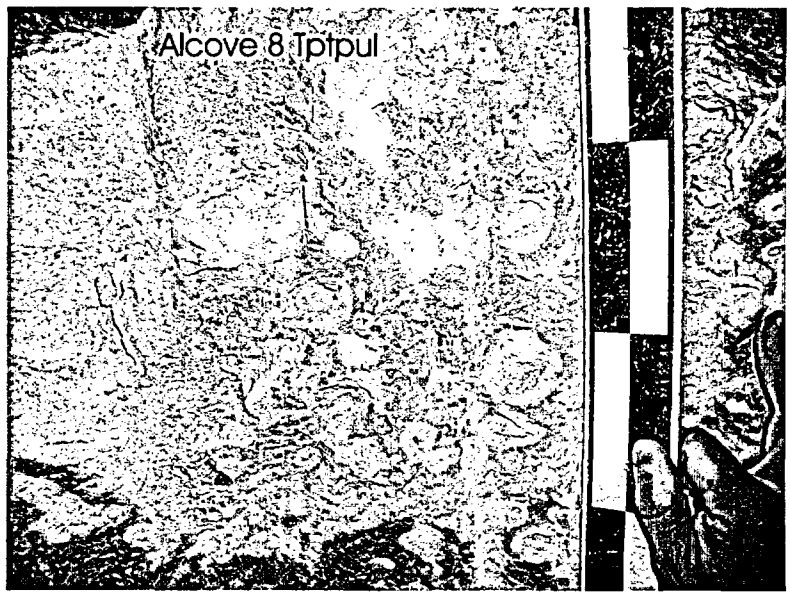

b)

NOTE: The core (top photo) was drilled with water, and the porous rims and fractures (many of which have rims) retain water and appear dark whereas the matrix-groundmass, which has minimal porosity, dries in a relatively short amount of time.

Figure 144. (a) Matrix Fracturing in the Tptpll in 12-in-Diameter Core and (b) Lack of Fracturing in Matrix of Tptpul as Seen in the Wall of Alcove 8 off the ECRB Cross-Drift

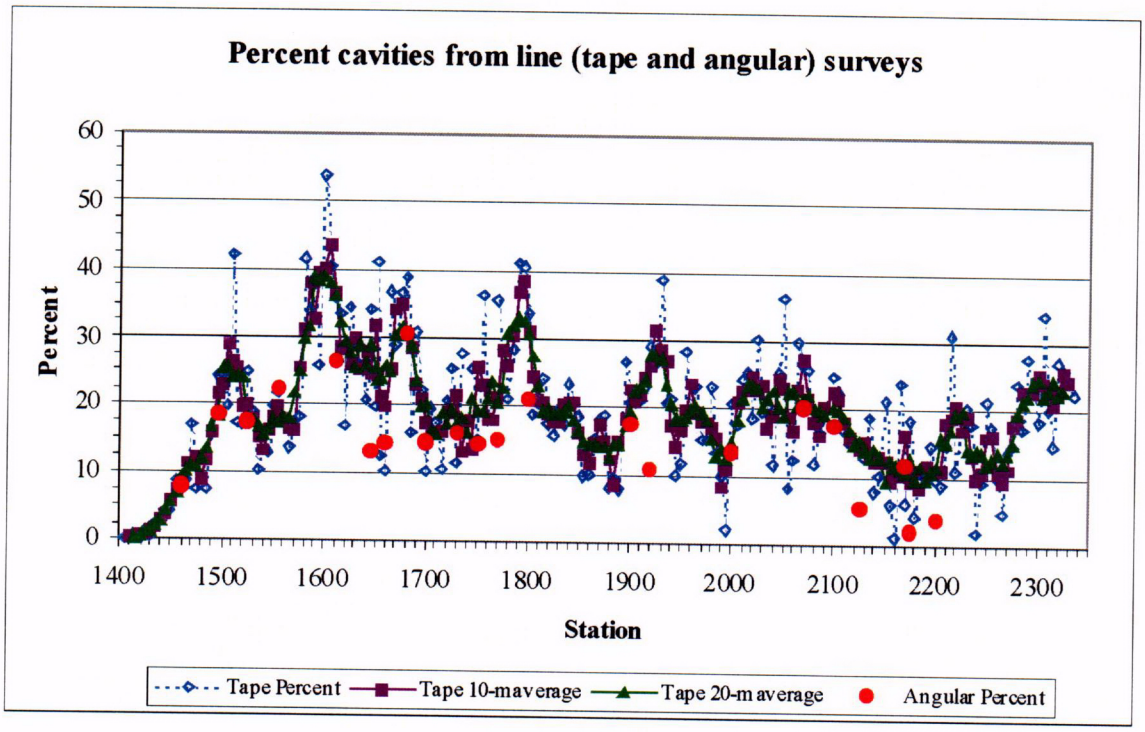

DTN: GS021008314224.002

Figure 145. Variation in Lithophysal Cavities in the Tptpll in the ECRB Cross-Drift from Top (Left) to Bottom of the Sub-Unit as Estimated by Tape and Angular Measurement Collected at 5-m Intervals

In general, the lithophysae diameter is much less than the diameter of the emplacement drifts (5.5 m). As shown in Figure 145, the variability of the porosity along the ECRB Cross-Drift is on the order of 5 m (additional data analysis is provided in Attachment XV). In representing the mechanical response of the lithophysal rocks, it is judged to be adequate to use a two dimensional, cross-sectional modeling approach in which the rock mass is considered to be of constant porosity, homogeneous and isotropic within that section.

7.3.2 Model Requirements for Drift Degradation Prediction

To represent drift degradation mechanisms and rockfall, the mechanical model and the numerical method in which it is embedded must have the following capabilities:

- The model must provide a general capability of modeling in situ stress, thermal and seismic loading of the rock mass.
- The model must represent the effects of porosity and matrix pre-existing fracturing on the elastic and strength properties of the material.
- The model must allow internal fracturing and detachment of the rock mass (i.e., rockfall) to occur in response to gravity, thermal effects, and seismic shaking.

C66

The above model requirements imply the necessity of use of a discontinuum approach to representation of the rock mass.

7.4 LABORATORY AND FIELD DATABASE FOR CONSTITUTIVE MODEL DEVELOPMENT AND MODEL VALIDATION

7.4.1 Database

A series of laboratory and field experiments have been conducted on lithophysal rocks to provide basic elastic and strength data for development of a mechanical material model. A large number of compression and tension tests have been conducted on small diameter (1-in to 2-in/25-mm to 50-mm) cores from the Tptpul and Tptpll. Several sets of data are available:

- Uniaxial compression and Brazilian tensile strength tests on 2-in (50-mm) cores from North Ramp geotechnical boreholes (DTNs: SNL02030193001.004; SNL02030193001.019; SNL02030193001.020)

- Uniaxial compression tests on 10.5-in (413-mm) diameter core samples of Tptpul from Busted Butte (Price et al. 1985) (DTN: MO0301RCKPRPCS.001)

- Uniaxial compression tests on 11.5-in diameter core samples from the Tptpul and Tptpll drilled from exposures in the ESF main loop and ECRB Cross-Drift (Attachment V, Table V-8) (DTNs: SN0208L0207502.001; SN0211L0207502.002)

- In situ slot uniaxial compression tests on 1 m rock samples of the Tptpul and Tptpll conducted in the walls and floor in the ESF main loop and ECRB Cross-Drift (Attachment V, Figure V-3) (DTNs: SN0208F4102102.002; SN0212F4102102.004; SN0301F4102102.006).

The small diameter cores do not accurately reflect the true strength or elastic properties of the lithophysal rock since the diameter precludes a reasonable sampling of the lithophysal voids. Therefore, reliance is placed on measurements from large samples that contain multiple lithophysal cavities in a given sample. The results of compression testing on samples from the Tptpul and Tptpll from the ESF main loop and ECRB Cross-Drift (Batch 1 and Batch 2) and from the Tptpul at Busted Butte (Price et al. 1985, DTN: MO0301RCKPRPCS.001) are provided in Attachment V (Table V-8).

Histogram plots of the room dry and saturated uniaxial compression strength and Young's modulus values from 24 tests given in Attachment V (Table V-8) are given in Figure 146a and b. The elevated temperature tests are not included in the statistical analysis of strength and modulus since the sample L:D ratios are much less than 2, thus resulting in an unknown confining (and strengthening) effect of specimen end friction. The mean unconfined compressive strength value for these tests is 17.8 MPa ± 6.5 MPa with a median value of 16.5 MPa. The mean Young's modulus is 10.1 GPa ± 5.3 GPa.

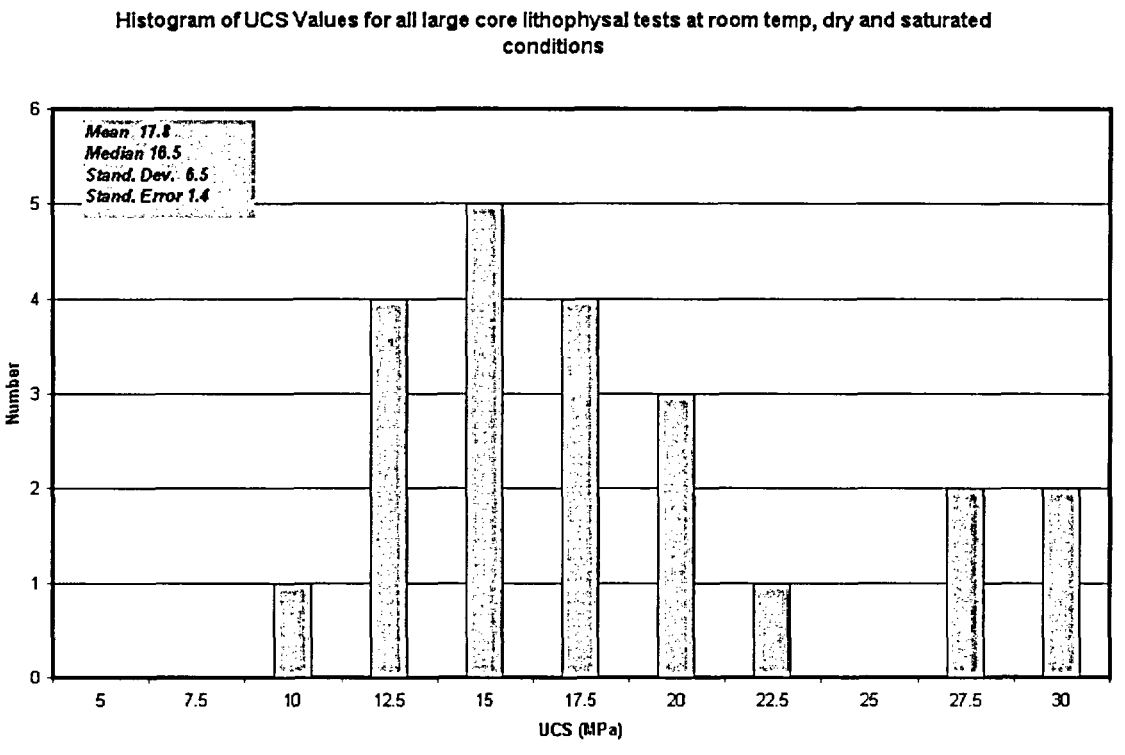

a)

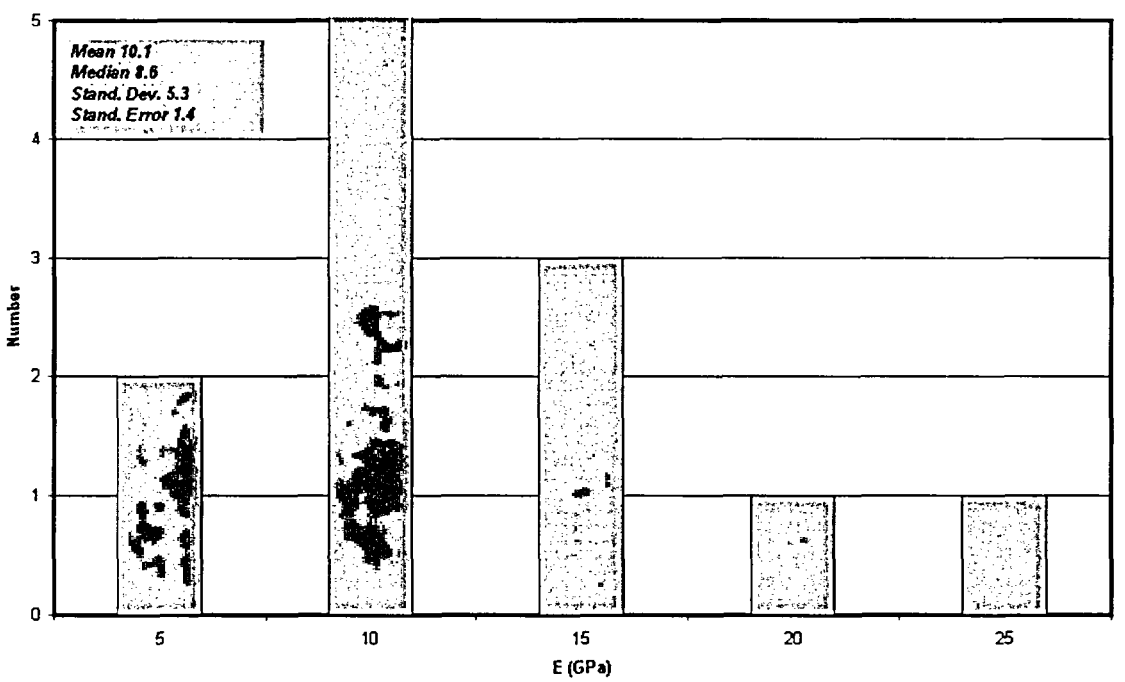

b)

NOTE: Source DTNs provided in Attachment V (Table V-8).

Figure 146. (a) Uniaxial Compression Strength Results for all Large Diameter Tptpul and Tptpll Core Samples from Batch 1 and 2 and Busted Butte and (b) Young's Modulus Measurements Batch 1 and Batch 2

The primary driver behind the variability in mechanical properties appears to be porosity variations in the samples as well as geologic unit (i.e., whether the sample was derived from the Tptpul or Tptpll). As shown in Figure 147, the lithophysal porosity of the room dry and saturated samples varies from approximately 12.5 to 30 percent with a mean value of 18.5 percent. This lithophysal porosity variation reasonably represents the range in in situ porosity as determined from surveys of the ECRB Cross-Drift tunnel surface (Figure 145). The unconfined compressive strength varies approximately logarithmically as a function of lithophysal porosity (Figure 148), and thus this data confirms the results of previous compression testing for all tuffs (Price et al. 1985).

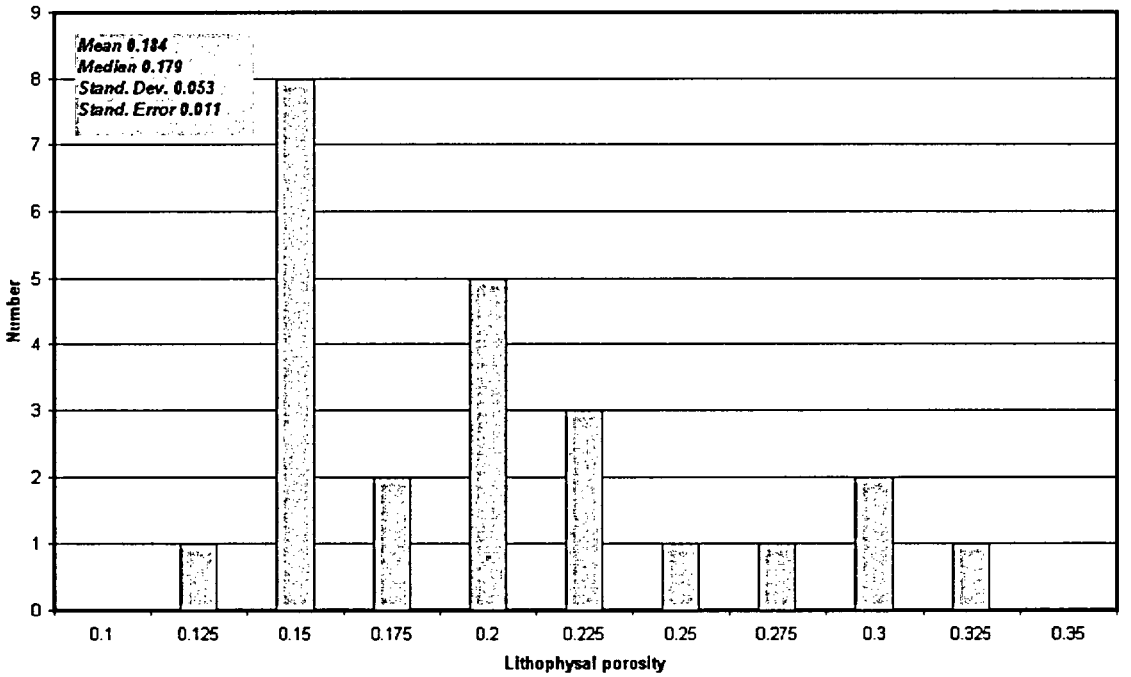

NOTE: Source DTNs provided in Attachment V (Table V-8).

Figure 147. Histogram of Estimated Porosities of Large Core Samples from Batch 1, Batch 2 and Busted Butte

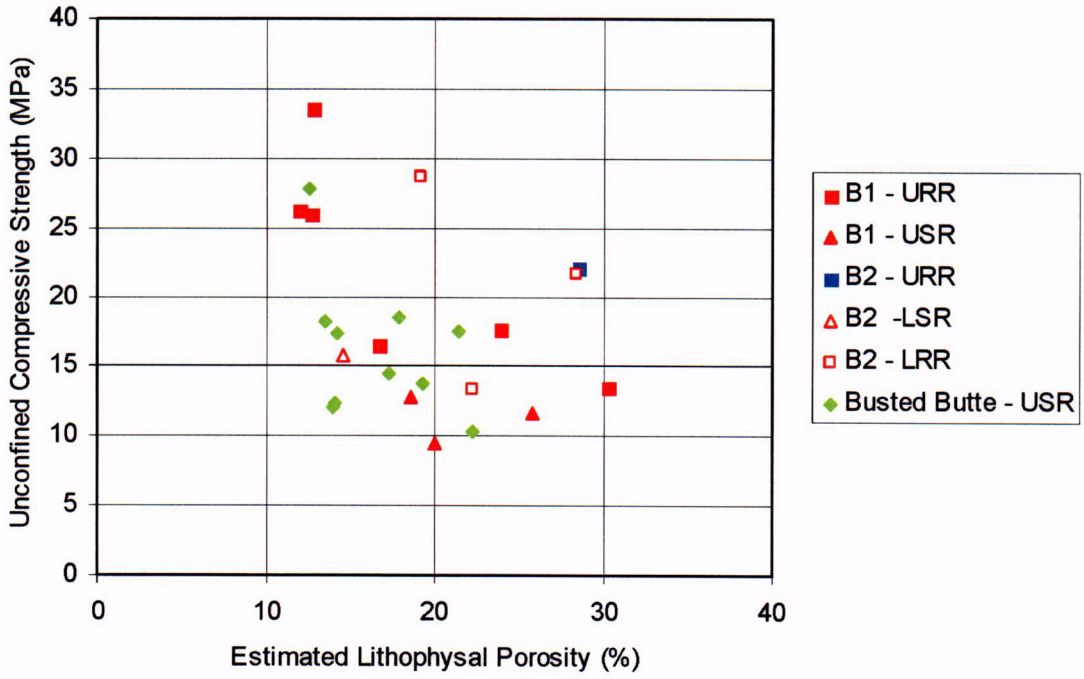

NOTE: Source DTNs provided in Attachment V (Table V-8). Legend notation defined in Attachment V (Figure V-3).

Figure 148. Variation of Unconfined Compressive Strength as a Function of Estimated Lithophysal Porosity from Batch 1, Batch 2 and Busted Butte Tptpul and Tptpll Large Core Samples

Since the unconfined compressive strength and Young's modulus do not vary independently from one another, it is convenient to present their ranges in the form of a single plot that demonstrates the relationship between their values (Figure 149). As seen here, the strength and stiffness varies approximately linearly for the entire Tptpul and Tptpll data set combined. The approximate values for the three in situ slot compression tests in the Tptpul and Tptpll (Attachment V, Figure V-3) are also given. Several observations regarding the laboratory results can be made:

- The unconfined compressive strength and Young's moduli vary approximately linearly, with a ratio of *E*/unconfined compressive strength of about 550 to 600. This ratio is generally consistent with other hard rocks (Goodman 1980).

- The primary mechanism for the range in laboratory test strength and moduli is the lithophysal porosity, following the general relations developed by Price et al. (1985).

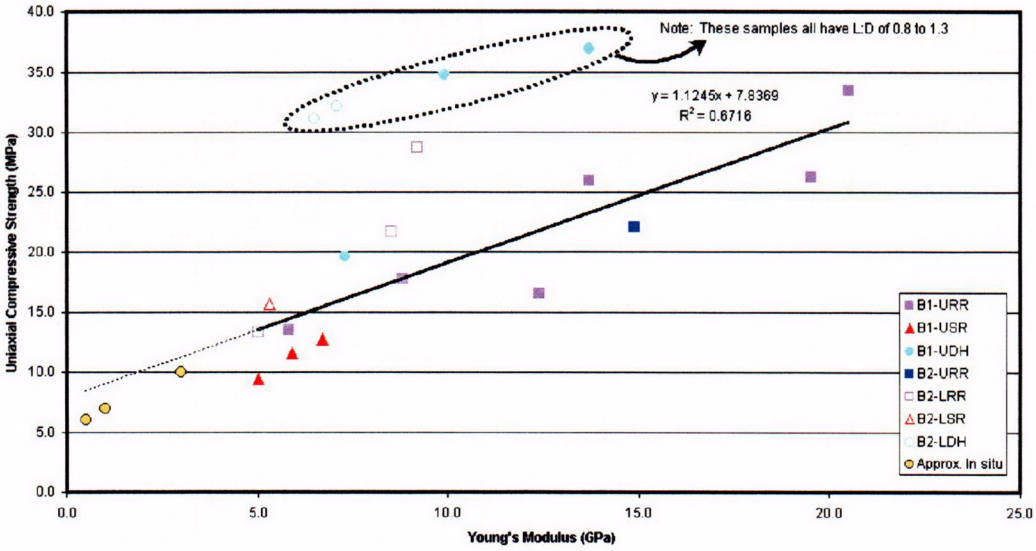

NOTES: Legend: B1/B2 = Batch 1 or 2; U=Tptpul; L=Tptpll; RR=room saturation, room temperature; SR=Saturated, room temperature; DH=dry, heated. Source DTNs provided in Attachment V (Table V-8). Samples with L:D ratios of less than 1.5 have been added for completeness, even though results are affected by confinement from specimen end restraints. In situ slot compression test results also shown for approximate comparison. The moduli are as calculated from field data. Strength is the failure stress of the sample, which may include some small confinement effects due to end restraints. Therefore, the resulting value is not strictly the uniaxial compressive strength.

Figure 149. Relationship of Uniaxial Compressive Strength to Young's Modulus for All Batch 1 and 2 Large Core Samples of Tptpul and Tptpll

The in situ slot compression tests show moduli and approximate strength values at the low end of the laboratory test data range. The lowest strength in situ test conducted in the poorest quality Tptpll near the contact with the Tptpmn was clearly in yielded ground in the sidewall of the ESF, and therefore, does not reflect true in situ values. However, it is clear that a significant size-effect exists in both the strength and modulus from the large core to 1-m sample dimensions. For example, in situ tests 2 and 3 in good quality Tptpul and Tptpll with estimated total porosity (lithophysal, rim, spot and matrix) of 24.3 and 21.9 percent, respectively, resulted in deformation moduli for the two tests of approximately 3 and 1 GPa, respectively.

7.4.2 Subdivision of Properties into Categories for Design and Performance Assessment Studies

The primary physical feature impacting rock quality conditions (and therefore rock mass strength and stiffness) in the lithophysal units appears to be the *lithophysal porosity*. As seen in Figure 149, the laboratory data shows a range in unconfined compressive strength from approximately 10 to 30 MPa with a corresponding range in Young's modulus from approximately 10 to 20 GPa. The estimated sample lithophysal porosity varies from approximately 10 to 30 percent over this range, or is roughly comparable to the range in situ values defined from mapping in the ECRB Cross-Drift (Figure 145). Thus, the core sampling used for the laboratory testing spans roughly the same range of lithophysal porosity (if not lithophysal size and shape) as observed throughout the ECRB Cross-Drift. The in situ testing indicates that a probable size effect also exists which

C68

extends the mechanical properties range down to a low-end strength of approximately 7 MPa and deformation modulus of approximately 1 GPa.

Since field data to confirm the exact nature of the lithophysal porosity and sample size effect are limited, a conservative engineering approach is used for defining input mechanical properties for the numerical modeling effort. The analysis method consists of conducting bounding parametric analyses of rock mass response to stressing (thermal, seismic and time-dependent degradation) using input data derived from the entire range of mechanical properties determined from the laboratory and field testing. Of course, it is realized that the in situ properties will be near the lower end of the property range.

For convenience, the mechanical rock properties range, as shown in Figure 149, is subdivided into six categories that cover the entire range of large-core laboratory testing and the in situ testing results. Table 45 presents these strength and moduli ranges derived by subdividing the laboratory data into five categories with an unconfined compressive strength increment of 5 MPa. The associated Young's modulus for each unconfined compressive strength is derived from the linear data fit given in Figure 149. The approximate equivalent lithophysal porosity for each of these ranges is given in Table 45. A sixth category, representing the in situ test data or lowest end of the property range is also given. It is considered that, by conducting numerical analyses with this entire range of data, that all levels of rock quality and rock mass response from lowest to highest porosity ranges and size effects can be covered.

Table 45. Suggested Range of Mechanical Properties Selected for Design and Performance Analyses

Category	Unconfined Compressive Strength (MPa)	Estimated Young's Modulus[a] (GPa)	Approximate Lithophysal Porosity From Laboratory Tests[b] (%)
1	10	1.9	25-30
2	15	6.4	20-25
3	20	10.8	15-20
4	25	15.3	10-15
5	30	19.7	<10
6[c]	6	1.0	Size effect represents ~ 20%

NOTES: [a]The calculation of Young's modulus values is documented in Attachment V (Section V.4.1).
[b]See Figure 148.
[c]Represents the in situ slot compression results in the Tptpll.
Source DTNs provided in Attachment V (Table V-8). UCS =.

7.5 STRATEGY FOR DEVELOPMENT OF A MECHANICAL MATERIAL MODEL FOR LITHOPHYSAL ROCKS

7.5.1 Continuum-Based Approach to Representing Rock Masses

The objective of the drift degradation analyses presented in this report is to predict the amount and particle size distribution of rockfall in the repository drifts due to stresses induced by the heat released by the emplaced waste, due to seismically related ground motions, and due to time-dependent strength loss of the rock mass. A standard approach for solving excavation stability problems in geotechnical engineering is the use of numerical models based on continuum mechanics (Figure 150). Such an approach is quite effective if the rock mass, in response to stressing, eventually arrives at a state of mechanical stability and where the primary purpose of the modeling is the computation of stress redistribution around an opening or determination of the final displacement profiles. However, difficulties are encountered if a continuum model is used for prediction of a mechanical system (i.e., a tunnel) that does not arrive at stable condition. Continuum models use constitutive relations to describe the mechanical behavior of a material. In rock, the mechanical effects of fractures and other features are "lumped" into the constitutive model, often using empirically based methods that take into account the spacing and continuity of the fractures, the roughness and alteration of the fracture surfaces, and the laboratory-determined properties of the intact rock blocks (e.g., Hoek 2000).

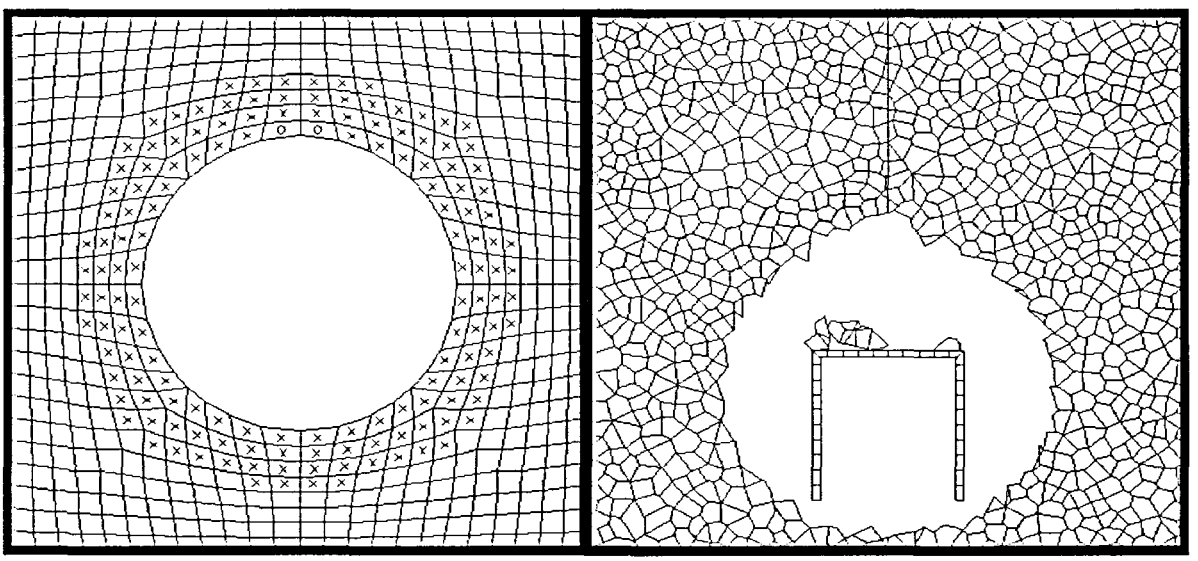

NOTES: The continuum approach models yield of the rock through use of a material model that enforces plasticity relations (note marked elements). Rock breakage and separation is not possible in this approach. The discontinuum approach also represents the rock mass using similar material models, but provides the capability for the rock mass to fracture and break apart on potential fracture surfaces.

Figure 150. Schematic Illustration of Continuum (Left) and Discontinuum (Right) Approaches to Modeling Drift Stability

A linearly elastic–perfectly plastic material model with Mohr-Coulomb yield criteria is a constitutive model often used to represent mechanical behavior of a rock mass. Because the material strength of a perfectly plastic, Mohr-Coulomb model does not decrease as a function of plastic deformation, this model will show indications of material yielding (i.e., plastic deformation) in different portions of the model, but will never actually predict the instability or rockfall. In order to be able to predict rockfall it is necessary to use some kind of strain-softening constitutive model, in which strength degrades as a function of deformation after the peak-strength of material has been reached. However, the strain-softening model, within the framework of continuum mechanics, is the subject of much research and debate, and not applicable with any degree of certainty to estimates of physical fracture and rockfall as required here. For this reason, continuum modeling methods are not used to represent rockfall.

7.5.2 Discontinuum Approach to Representing Rock Masses

The estimation of rockfall requires that the modeling technique and mechanical material model be capable of representing physical fracture of the rock mass and separation of the intact rock mass into blocks of material. In particular, an estimate of the size distribution of particles is desired. This requires the use of a discontinuum numerical method (i.e., a method in which slip and separation of contacting rock blocks can be estimated [Figure 150]). The following strategy is based on use of discontinuum methods for development of a material model for lithophysal rocks.

7.5.3 Strategy for Discontinuum Material Model Development

Typically, development of a mechanical material model for a rock mass is based on extensive laboratory testing of rock core, determination of strength and moduli reduction factors via in situ mapping of rock quality, followed by validation against field measurement. Such an approach to development of a material model for the lithophysal rocks presents a number of challenges. As discussed in the previous section, it is problematic to conduct an extensive mechanical properties testing program on lithophysal rocks due to the need to obtain and test large cores or to create large in situ samples from sawing or drilling. Additionally, direct determination of the true triaxial stress behavior of samples is difficult since pressure vessels to provide confinement to large core samples are not available. It is also not possible to conduct testing on a wide range of lithophysae shapes and size distributions. Finally, geotechnical classification systems are not particularly applicable to the lithophysal rocks due to a lack of contemporary experience in construction and testing in this type of rock mass.

As described previously, the database available for model development includes: 1) uniaxial and triaxial compression and direct pull tensile testing of nonlithophysal rock; and, 2) uniaxial compression testing of large scale cores and in situ blocks of lithophysal tuff. To overcome these sampling and testing limitations, an alternative strategy is used here, as illustrated in Figure 151. In this section, an approach is described in which a physics-based "micromechanical," discontinuum numerical modeling program—the Particle Flow Code (PFC) program (Itasca 2002; Potyondy and Cundall 2001)—is used as a numerical "laboratory" to simulate and test the basic deformation and failure response mechanisms of lithophysal tuff. The PFC program was chosen due to its ability to simulate the physics of deformation and fracture of a bonded granular matrix that contains void space of varying shape, size and porosity. The

program is first validated against the existing laboratory compression data. Specifically, it is demonstrated that a detailed understanding of the basic physical mechanisms of the rock mass behavior can be obtained without resorting to empiricism or complex constitutive modeling. The model is then used to extend the laboratory data by conducting numerical experiments on simulated samples of lithophysal tuffs at various physical conditions of porosity, lithophysae shape and distribution, as well as various levels of confinement and applied stress. From this modeling, it is possible to understand the size-scaling and variability issues introduced by lithophysae shape and distribution, and their impact on rock mass properties and failure criteria.

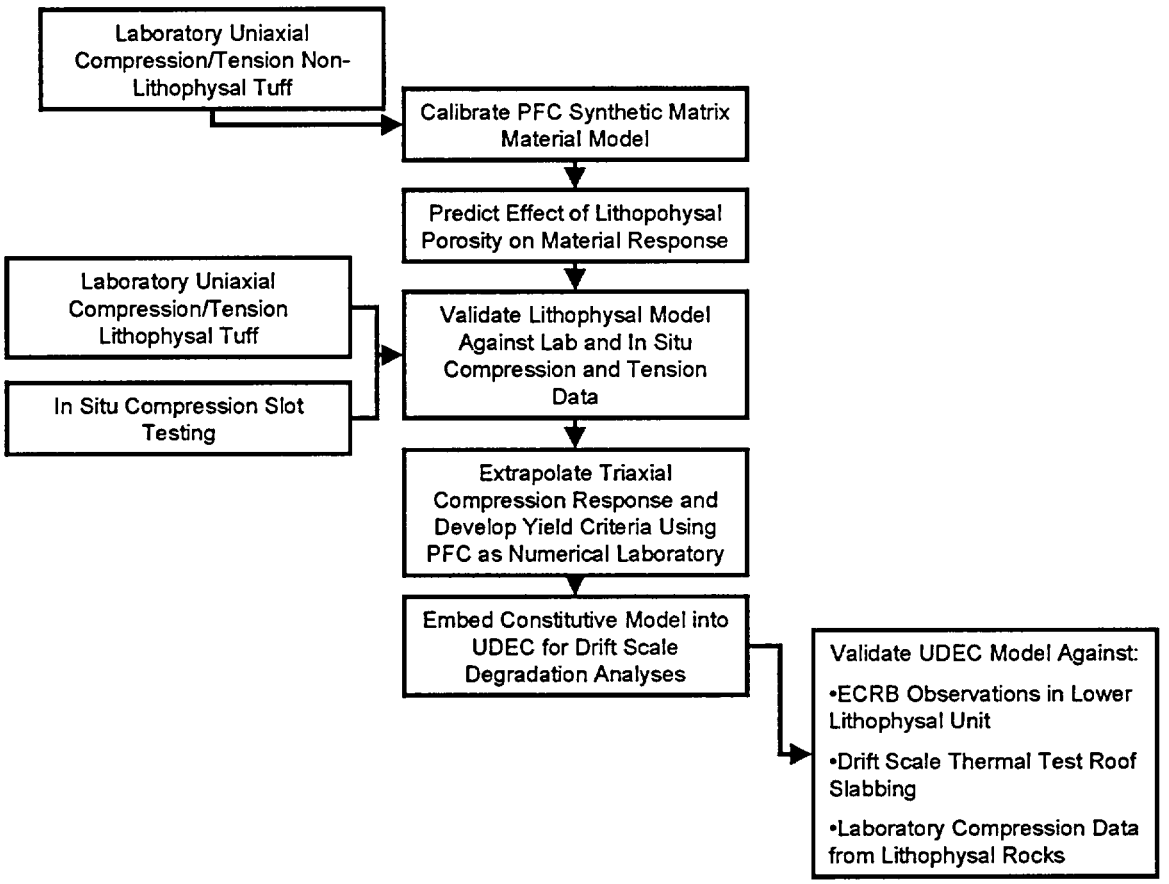

Figure 151. General Approach to Validation of Mechanical Material Model for Lithophysal Rocks

Although possible, it is impractical to use the PFC program as a general modeling tool to investigate drift degradation due to the extensive computing demands that result from large-scale problems. Instead, the material model developed from the testing and PFC extrapolation is embedded in the UDEC discontinuum program, which has been used efficiently to examine tunnel-scale seismic, heating and time-degradation issues.

7.6 VALIDATION OF THE PARTICLE FLOW CODE (PFC) - A MICROMECHANICAL MODEL REPRESENTATION OF THE MECHANICAL BEHAVIOR OF LITHOPHYSAL ROCK

7.6.1 The PFC Model

The Particle Flow Code has been qualified for use as indicated in Section 3. The PFC approach (Figure 152) represents rock as a number of small, rigid, spherical grains that are bonded together at their contacts with a shear and tensile strength, as well as a grain to grain friction angle after the "contact bond" has been broken. If cementing exists between grains, it can be represented with a "parallel bond" that provides a rotational resistance as well. Details on the mechanics of the PFC program are provided in *Itasca Software–Cutting Edge Tools for Computational Mechanics* (Itasca 2002). The deformability of the contacts between particles is represented by a normal and shear stiffness at the contact point. Porosity is developed naturally in the model by control of the shape and size of void space between chains of bonded grains. The contact properties and porosity distribution are referred to as "microstructural" properties. Thus, the input conditions necessary for the model are very simple, only contact strength and stiffness. However, as shown below, extremely rich constitutive behavior may develop *naturally* based on porosity and the few straightforward input properties and their variability throughout the rock.

When load is applied to the grain assembly, forces are transmitted across contacts. If the shear or tensile strength of the contact is reached, failure will occur, and the adjacent particles are free to slide past one another, or to separate. In either case, a fracture is formed and the forces must reorient in some fashion, thus redistributing loads. Realistic failure mechanisms may then develop which can be compared to those observed in the laboratory. Calibration of the model against laboratory testing is necessary via sensitivity studies in which the contact strength and stiffness values are varied and the macroscopic stress-strain response is compared to that monitored.

7.6.2 Comparison of PFC Model Results Against Compression and Tensile Laboratory Tests on Cores

A discussion of the PFC calibration and extrapolations is provided in this section, including a summary of the approach and results. The PFC program in both two- and three-dimensions was "calibrated" first against laboratory strength tests of nonlithophysal rocks. Since it is considered that the matrix or groundmass material of the Tptpul, Tptpmn, and Tptpll is essentially the same, both mineralogically and mechanically, it is necessary to first make certain the PFC model can represent the mechanical response of the material without lithophysal voids. Once the matrix material response is identified, then representation of the mechanical behavior of the lithophysal material should simply be possible with the simple addition of void space (assuming the consideration of similar matrix is correct).

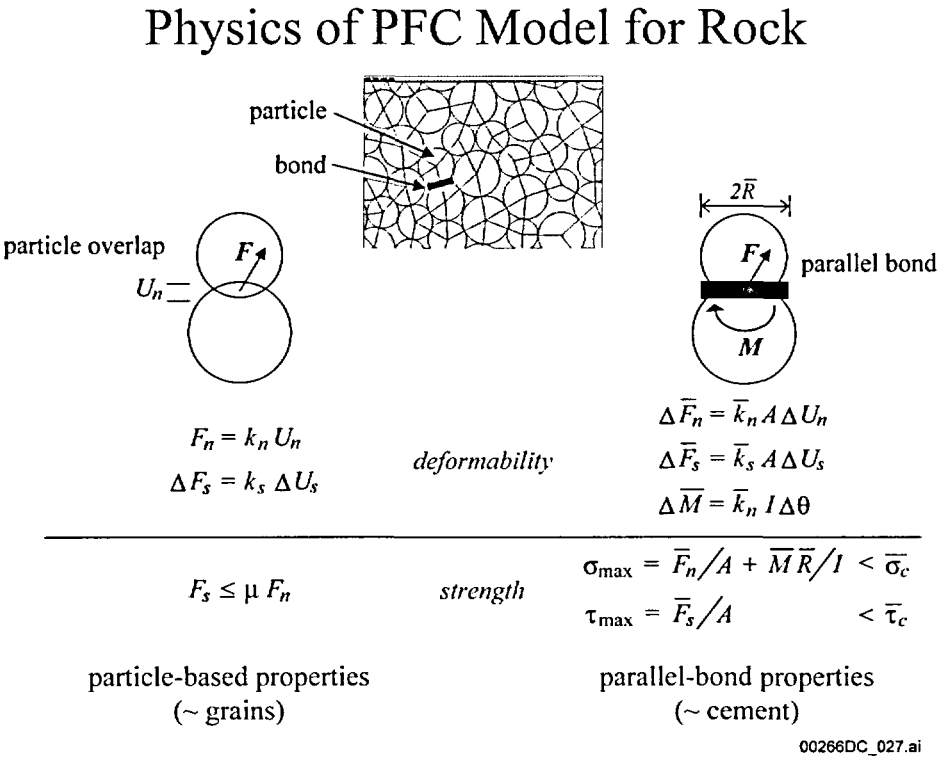

NOTES: Mechanical response in the PFC program is governed by the strength and deformability relationships of the bonds between rigid particles. Two bond types are provided: a simple contact bond (left), and a parallel bond (right), which simulates cement between particles that resists moments as well as shear and normal loads.

F_n = normal contact force
k_n = normal stiffness
U_n = relative normal displacement
ΔF_s = shear contact force increment
k_s = shear stiffness
ΔU_s = relative shear displacement increment
$\Delta\overline{F}_n$ = axial-directed force increment for bond
$\overline{k}_n$ = bond normal stiffness
A = area of bond cross-section
ΔU_n = relative normal displacement increment
$\Delta\overline{F}_s$ = shear-directed force increment for bond
$\overline{k}_s$ = bond shear stiffness

ΔU_s = relative shear displacement increment
$\Delta\overline{M}$ = bending moment increment for bond
I = moment of inertia of the bond cross-section
$\Delta\theta$ = increment of rotational angle
F_s = shear contact force
μ = contact friction coefficient
σ_{max} = maximum tensile stress acting on the bond periphery
τ_{max} = maximum shear stress acting on the bond periphery
$\overline{R}$ = particle radius
$\overline{F}_n$ = axial-directed force for bond
$\overline{F}_s$ = shear-directed force for bond

Figure 152. The Basic Mechanics of the PFC Program

The tuff can be divided into lithophysal and nonlithophysal types. These two rock types differ significantly in their microstructural and mechanical properties. In the lithophysal tuff, the vast majority of the porosity is concentrated in lithophysae and surrounding vapor-phase altered material, whereas in the nonlithophysal tuffs porosity is more evenly distributed throughout the material. The nonlithophysal tuffs have effective porosities that increase from 0.12 to 0.38 as the extent of welding decreases. The high-porosity nonlithophysal tuffs have large effective porosities because of the voids between grains, whereas similar effective porosities in lithophysal tuffs arise from the presence of lithophysae and vapor-phase altered material. The matrix fabric of the lithophysal tuff is microscopically identical to that of moderately to densely welded nonlithophysal tuff. Price et al. (1985) divide the lithophysal tuff into the following three components: a fine-grained matrix (*M*), large lithophysae (*L*), and vapor-phase altered material (*A*) surrounding the lithophysae. Based on the approach described by Price et al. (1985) for determining bulk properties of lithophysal tuff, the porosity of component-i is denoted by

$$\phi_i = \frac{(V_v)_i}{V_i}, \qquad i = \{M, A, L\} \qquad \text{(Eq. 13)}$$

and the volume fraction of component-i by

$$P_i = \frac{V_i}{V}, \qquad i = \{M, A, L\} \qquad \text{(Eq. 14)}$$

where $(V_v)_i$ is the void volume of component-i , V_i is the solid volume of component-i and V is the total volume. The total porosity can be expressed as

$$\phi = \frac{(V_v)_M + (V_v)_A + (V_v)_L}{V} = \phi_M P_M + \phi_A P_A + \phi_L P_L \qquad \text{(Eq. 15)}$$

The PFC material models lithophysal tuff as a base material with discrete voids. The base material represents both the matrix (*M*) and the vapor-phase altered material (*A*) in a smeared fashion, and the discrete voids represent the lithophysae (*L*). The void porosity, n_v, defined by Equation 13, of the PFC model corresponds with the volume fraction, P_i, of the lithophysal tuff. The relative distributions of these components for the lithophysal tuff and the PFC model are shown in Figure 153. Note that the PFC base material has an inherent porosity (approximately 0.17 and 0.36, for PFC2D and PFC3D, respectively) that does not correspond with that of the tuff; the tuff microstructure at this small-scale is not reproduced by the PFC material. Only the void porosity of the PFC material can be compared with the lithophysal volume fraction. Also note that P_A as a function of P_L is not known, but P_A must approach zero as P_L approaches zero. The microproperties of the PFC material are kept constant for all values of $n_v = P_i$, and thus, the PFC materials with low void porosity are overestimating the weakening effect of the vapor-phase altered material. One approach to incorporate this effect in the PFC models would be to modify the PFC microproperties as a function of n_v such that they match the laboratory data for the lithophysal tuff in the non-zero range of n_v and match the nonlithophysal tuff when $n_v = 0$. This approach has not been adopted here.

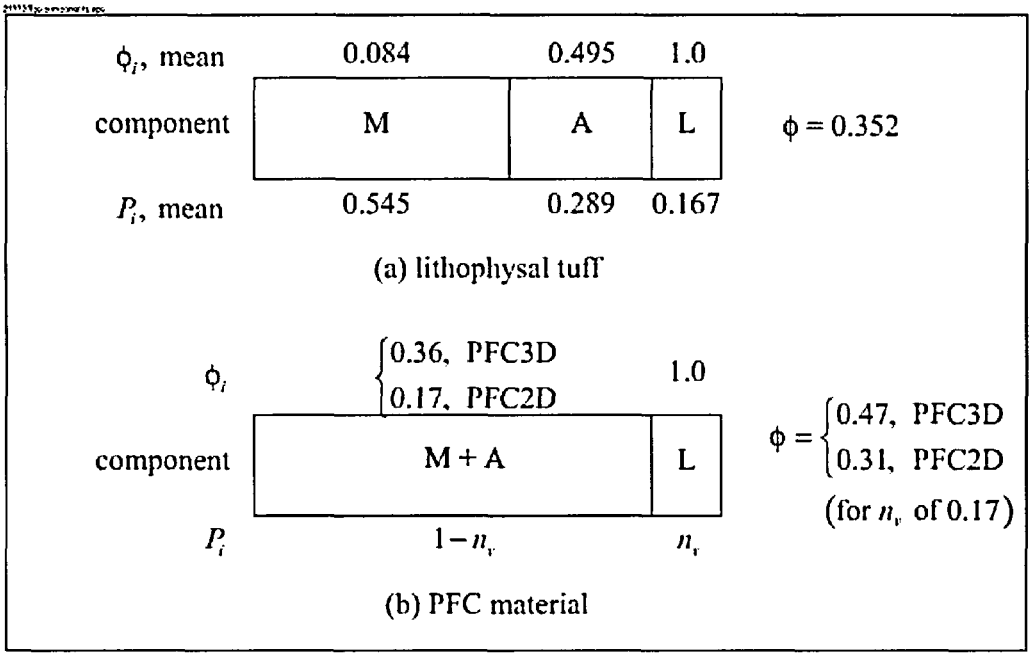

Figure 153. Relative Distributions of the Three Components of Lithophysal Tuff for (a) Real Material (Price et al. 1985) and (b) PFC Materials

The void-filled PFC material can be calibrated by matching the variation of modulus and strength with volume fraction of lithophysal tuff. The laboratory data used for calibration is that shown in Attachment V (Table V-8). The nonlithophysal tuff exhibits a size effect such that larger specimens are weaker with unconfined compressive strength values ranging from approximately 190 to 90 MPa as specimen diameter ranges from 25 to 230 mm (Price 1986). The form of a size effect for lithophysal tuff has not been identified, but is considered to be similar to that of the nonlithophysal tuff. The effect of specimen size is not investigated for the PFC models; instead, all PFC models are either 1:1 or 2:1 aspect ratio specimens of one-meter diameter, and microproperties are chosen to match the laboratory data.

7.6.3 Calibration of PFC Model Properties

7.6.3.1 Laboratory Test Simulation

The PFC2D and 3D models were calibrated against laboratory data from large diameter testing of Busted Butte initially, and then compared to recently obtained compression test data from the Batch 1 and Batch 2 as described previously. The general procedure used was to use PFC to conduct simulated laboratory compression tests on samples of lithophysal rocks with various void porosities. The microproperties of the PFC model are adjusted to achieve a match to the unconfined compressive strength and Young's modulus variation as a function of lithophysal porosity. A further check against the model is performed by examining the subsequent relation between unconfined compressive strength and Young's modulus (i.e., these mechanical properties are not independent of one another and thus the model must achieve a reasonable match to strength and stiffness and the relationship between them). Additionally, the mode of failure of rock samples in compression must be similar to that observed in the laboratory.

Figures 154 to 155 show PFC2D and 3D models of several rock samples at increasing void ratios that are used to conduct numerical laboratory experiments. Particles are removed to create circular or spherical voids with random location.

Examples of uniaxial compression simulations for nonlithophysal and lithophysal samples with void porosities of 0, 10 and 20 percent are shown in Figures 156 to 158. The models show numerous physical features that correspond to observed laboratory response. The nonlithophysal samples fail through formation of conjugate shear fractures composed of coalescing tensile bond breakages. The response is highly elastic to the point of brittle failure (i.e., there is little observable hysteresis on load-unload cycles directly up to the yield limit). This behavior is a function of the uniform grain structure and welding of the matrix material. The addition of lithophysal voids results in significant decreases in both the strength and modulus. The failure mechanism in this case is a function of tensile splitting between adjacent lithophysal voids due to induced tensile stresses in the thin webbing between voids. Essentially, the PFC model shows that the failure strength is simply governed by the ratio of void span to webbing thickness. With voids randomly distributed, the thinnest of webbing will fail first, shunting load to other solid webs, resulting in progressive failure of the weakest "link." The resulting stress-strain behavior becomes less brittle in nature due to this progressive failure mode.

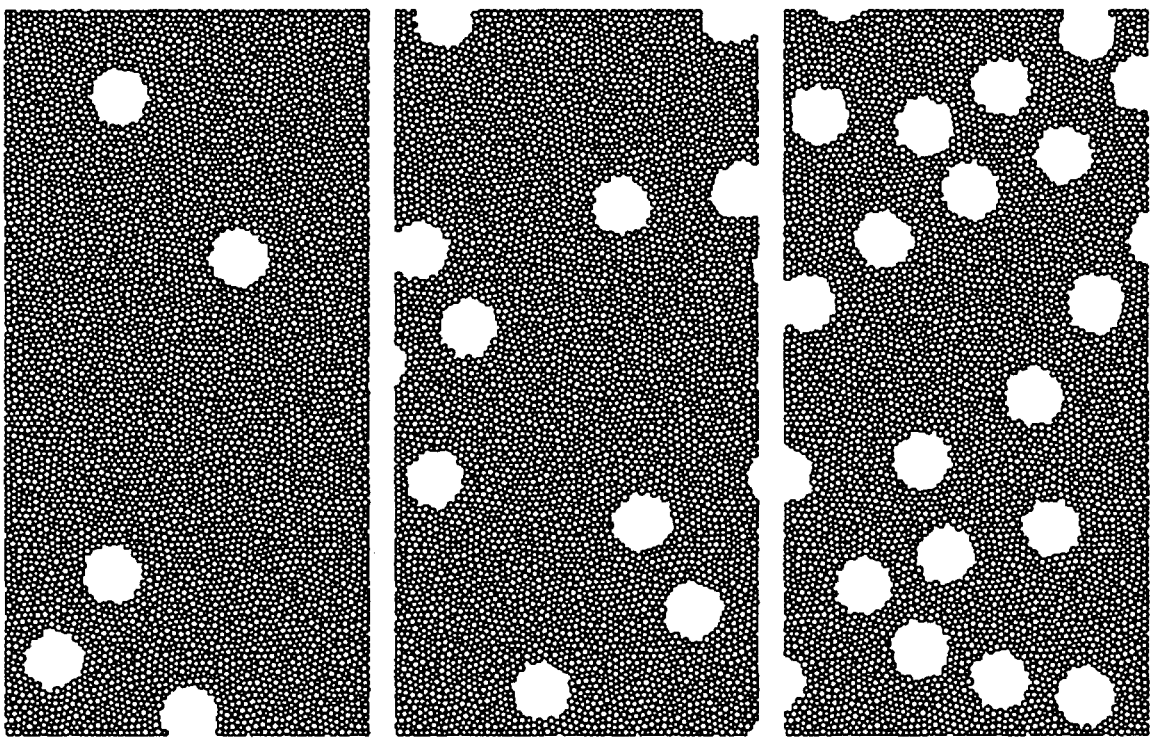

NOTES: Circular Voids; Radius = 83 mm; nv = 0.05, 0.10, and 0.20.

Figure 154. PFC2D Unconfined Compressive Strength Test Specimens

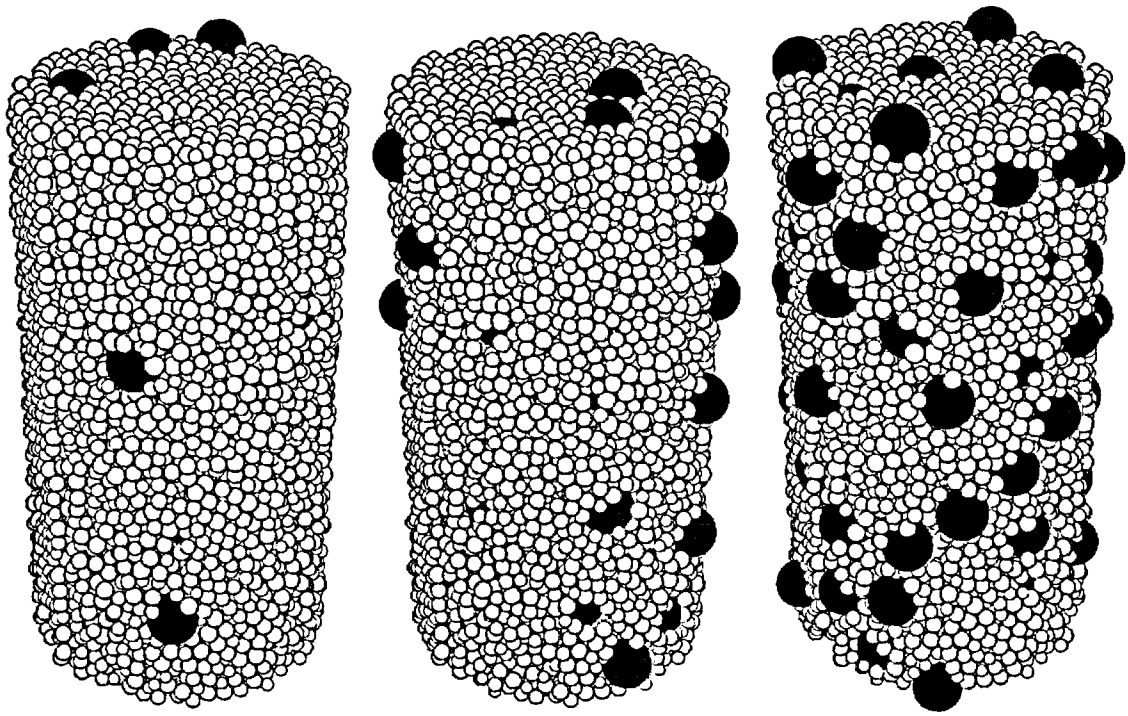

NOTES: Spherical voids; Radius = 83 mm; n_v = 0.05, 0.10, and 0.20.

Figure 155. PFC3D Unconfined Compressive Strength Test Specimens

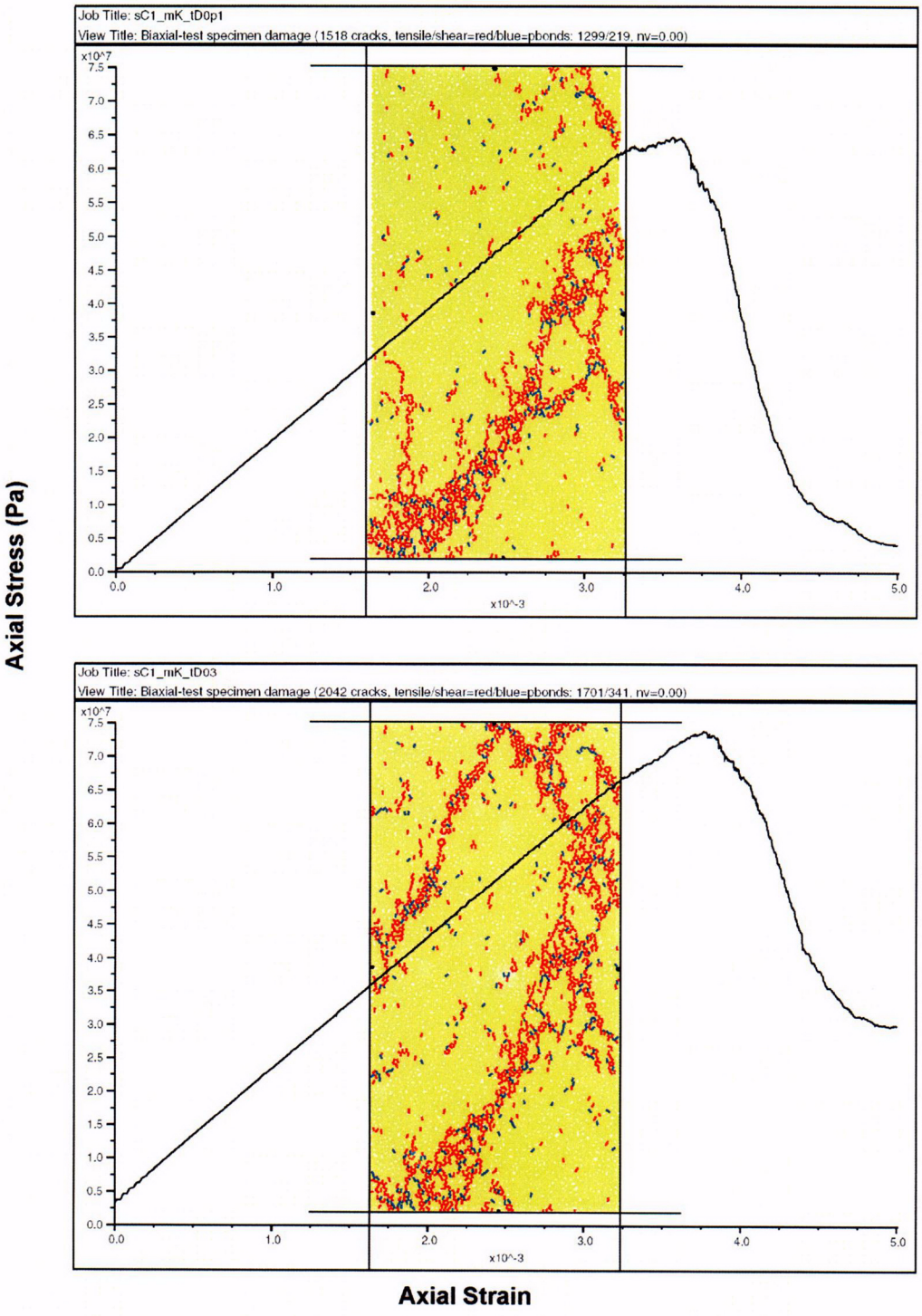

NOTES: Final sample damage state is plotted with bond failures in tension (red) and shear (blue). Samples fail with typical conjugate shear fractures. Two confining pressures are shown: 0.1 MPa (top) and 3 MPa (bottom). The primary impact of confinement is slightly increased peak and residual strength.

Figure 156. PFC2D Simulation of Confined Compression of 2:1 L:D Samples of Nonlithophysal Material (n_v = 0) Composed of Several Thousand Bonded Particles

C69

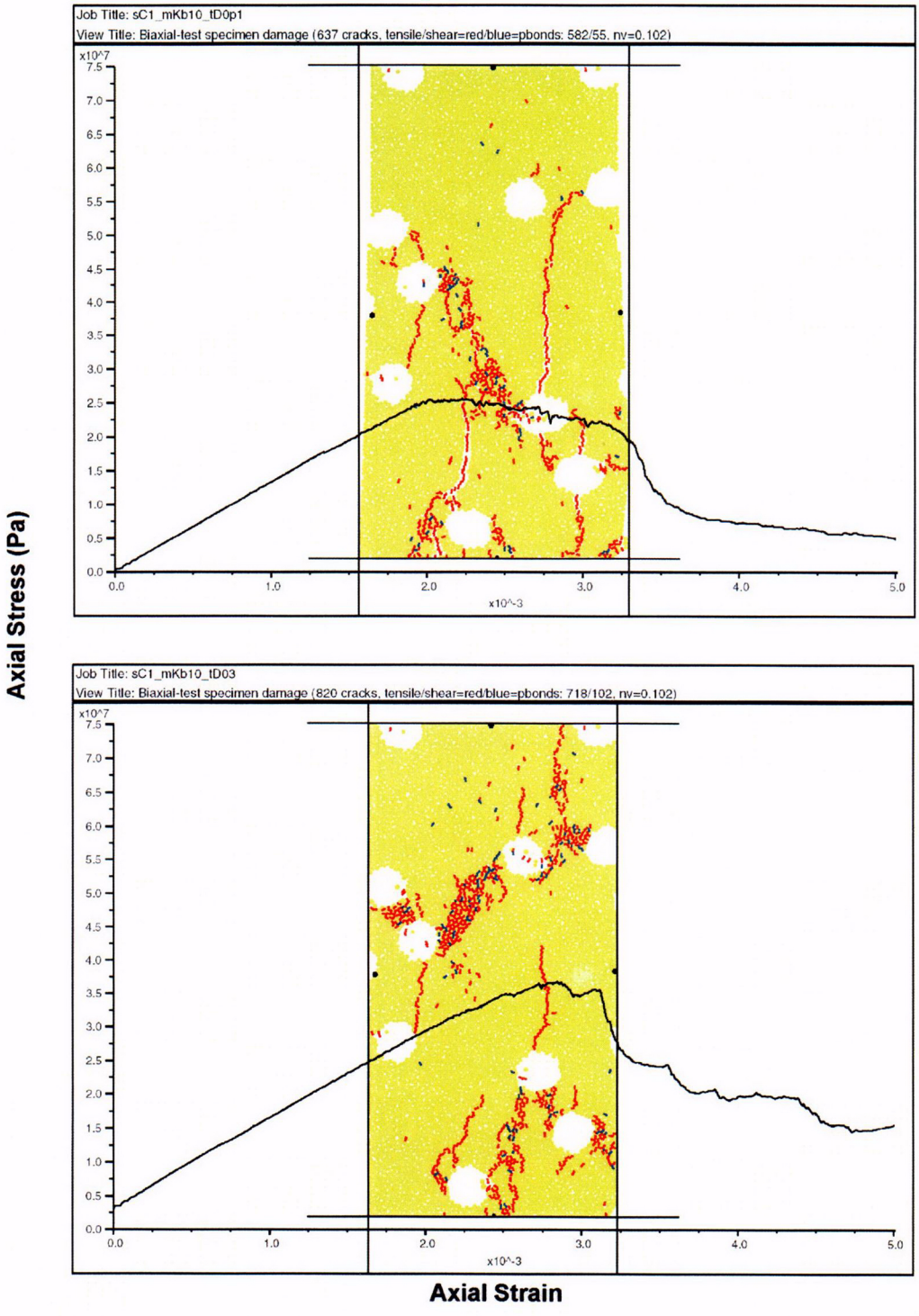

NOTES: Final sample damage state is plotted with bond failures in tension (red) and shear (blue). Two confining pressures are shown: 0.1 MPa (top) and 3 MPa (bottom). Samples fail in an axial splitting mode which is most pronounced in the low confinement model at left. Note that confinement increases peak strength with increased residual strength.

Figure 157. PFC2D Simulation of Confined Compression of 2:1 L:D Samples of Lithophysal Material (n_v = 0.10) Composed of Several Thousand Bonded Particles

C70

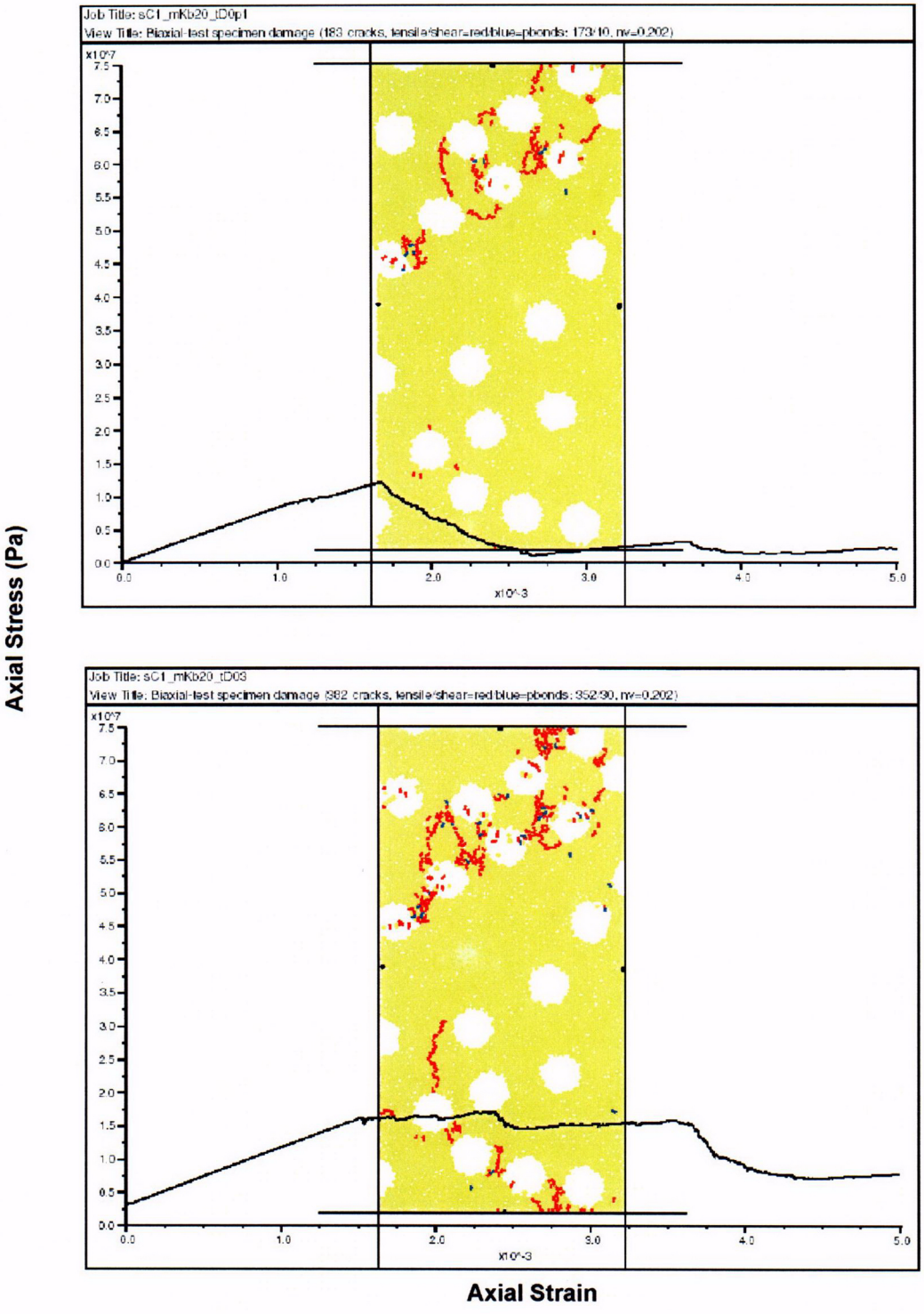

NOTES: Final sample damage state is plotted with bond failures in tension (red) and shear (blue). Two confining pressures are shown: 0.1 MPa (top) and 3 MPa (bottom). Samples fail due to tensile splitting between adjacent voids in the low confinement model at left. Note that confinement results in a slight increase in peak strength with increased residual strength at high values of void porosity.

Figure 158. PFC2D Simulation of Confined Compression of 2:1 L:D Samples of Lithophysal Material (n_v = 0.20) Composed of Several Thousand Bonded Particles

The impact of lithophysae on direct tension strength follows the same general mechanism: the voids result in less area of solid rock for any given cross-section (Figure 159). For a constant applied force, the stress in the remaining solid will be higher, thus reducing the overall averaged tensile strength of the sample. Particles are removed to create circular or spherical voids with random location subject to the constraint that no two voids are closer than one-half of the void radius.

7.6.3.2 Validation of PFC - Ability to Reproduce Observed Laboratory Mechanical Data and Impact of Lithophysal Void Porosity

The properties of the Batch 1 and Batch 2 lithophysal tuff samples from the ESF main loop and ECRB Cross-Drift (Attachment V, Table V-8) are plotted along with those of the best-fit PFC materials in Figures 160 to 161, which includes the relation between Young's modulus and strength. Both PFC materials provide a reasonable match to the Batch 1 and Batch 2 data. The slopes of the PFC2D material are greater than the corresponding slopes of the PFC3D material, which indicates that the PFC2D material is more sensitive to void porosity than is the PFC3D material. Both PFC materials match the modulus-strength relation of the lithophysal tuff (Figure 162).

7.6.3.3 Conclusion from PFC Model Validation - Comparison to Criteria

The above PFC studies have shown the following:

1. The PFC model is able to reproduce the basic failure mechanisms observed in the laboratory for nonlithophysal and lithophysal rocks (lithophysal rock validation criteria B, Section 7.2.2).

2. The model provides information that allows understanding of the detailed mechanism of failure in lithophysal rocks and accounts for the strength and moduli reduction mechanism with increasing lithophysal void percentage. The presence of voids in a sample under compression creates stress concentrations around the voids, promoting tensile splitting phenomena between voids. The result is a weakening effect that increases as a function of increasing void volume, and decreasing web thickness between voids (lithophysal rock validation criteria B, Section 7.2.2).

3. The strength and modulus reduction with void porosity predicted by the model compares reasonably well with that observed in the laboratory. Thus, the PFC model is able to capture the impact of lithophysal porosity variability on strength and deformability properties (lithophysal rock validation criteria (a), Section 7.2.2).

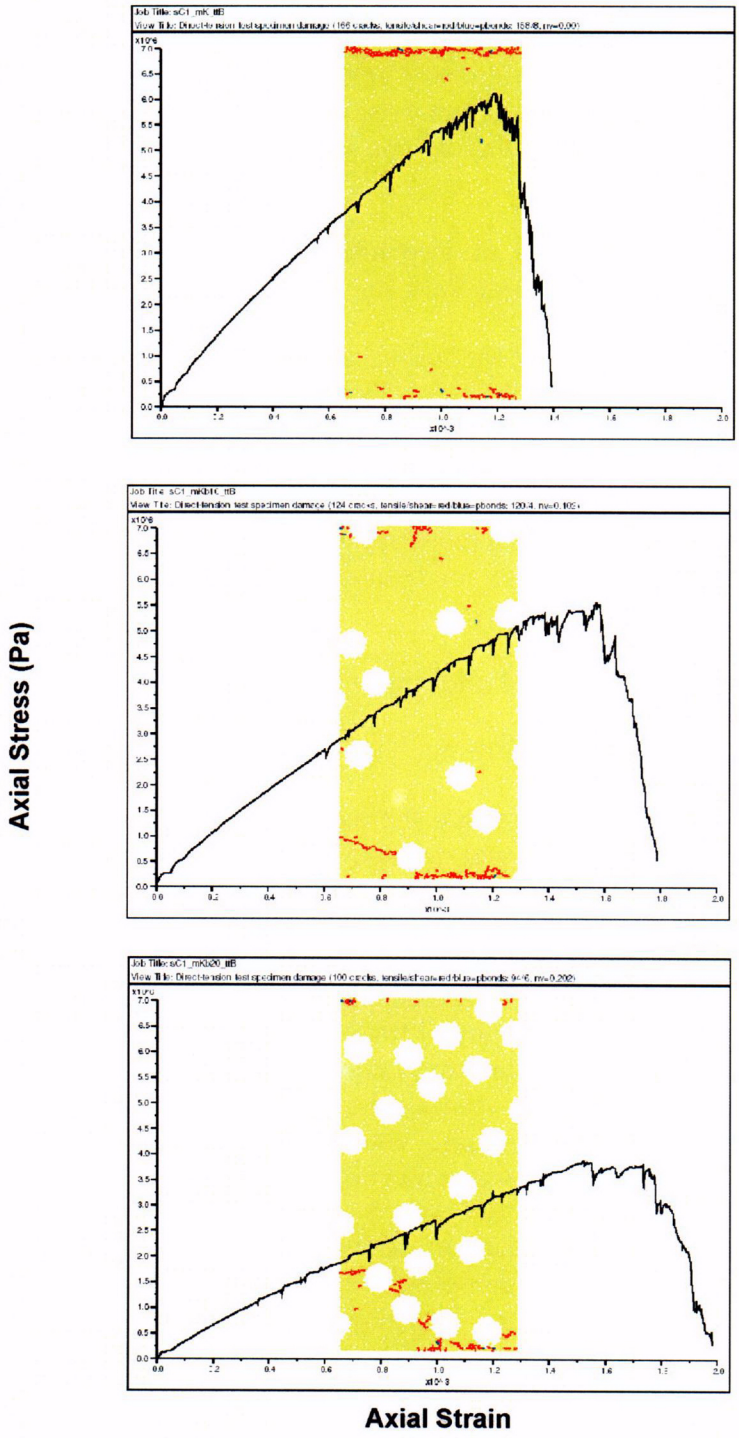

NOTES: Final sample damage state is plotted with bond failures in tension (red) and shear (blue). The effect of increasing lithophysal voids is to reduce the amount of solid rock that must fail in tension across any cross-section, thus reducing the overall tensile strength of the body. The body fails at the cross-section with minimum solid.

Figure 159. PFC2D Simulation of Direct Pull Strength of 2:1 L:D Samples of Nonlithophysal and Lithophysal (n_v = 0.10 and 0.20) Composed of Several Thousand Bonded Particles

CTZ

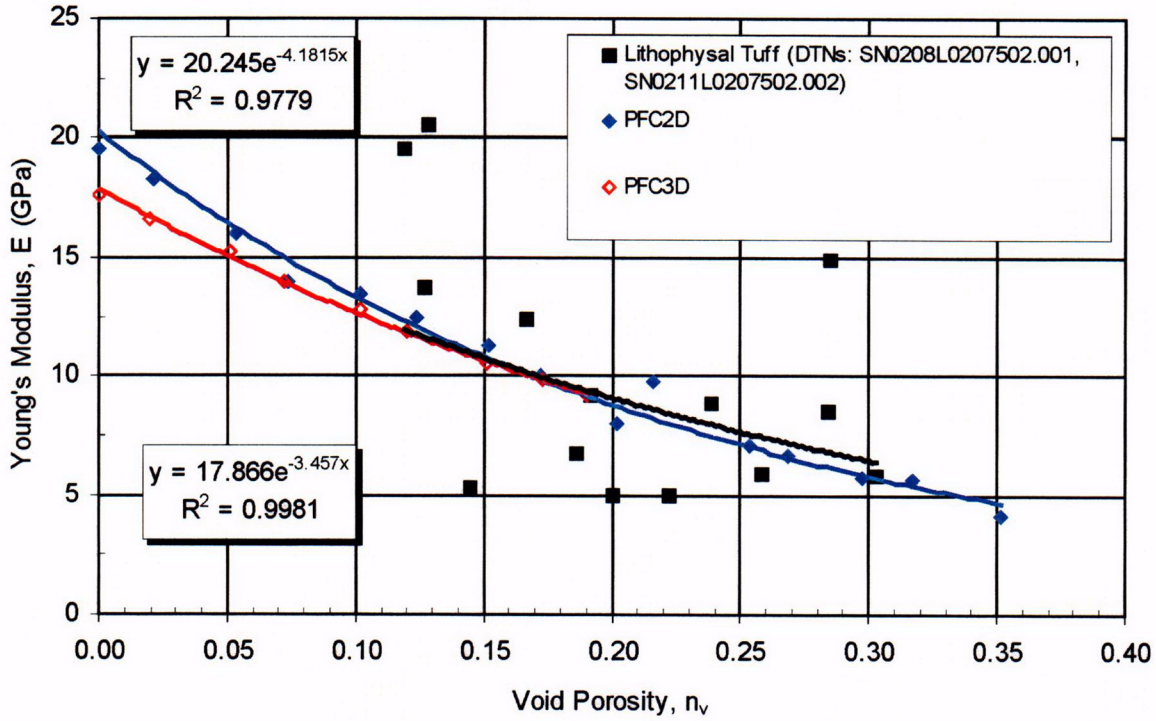

Figure 160. Young's Modulus Versus Void Porosity for Lithophysal Tuff and PFC Materials

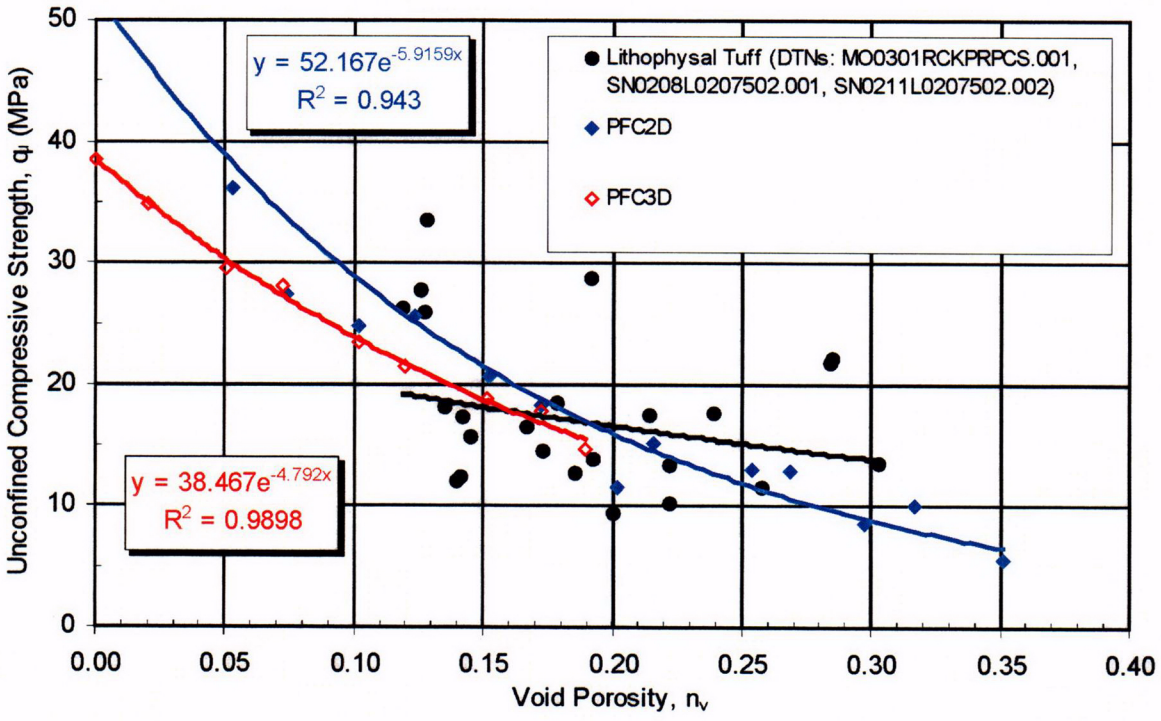

Figure 161. Unconfined Compressive Strength Versus Void Porosity for Lithophysal Tuff and PFC Materials

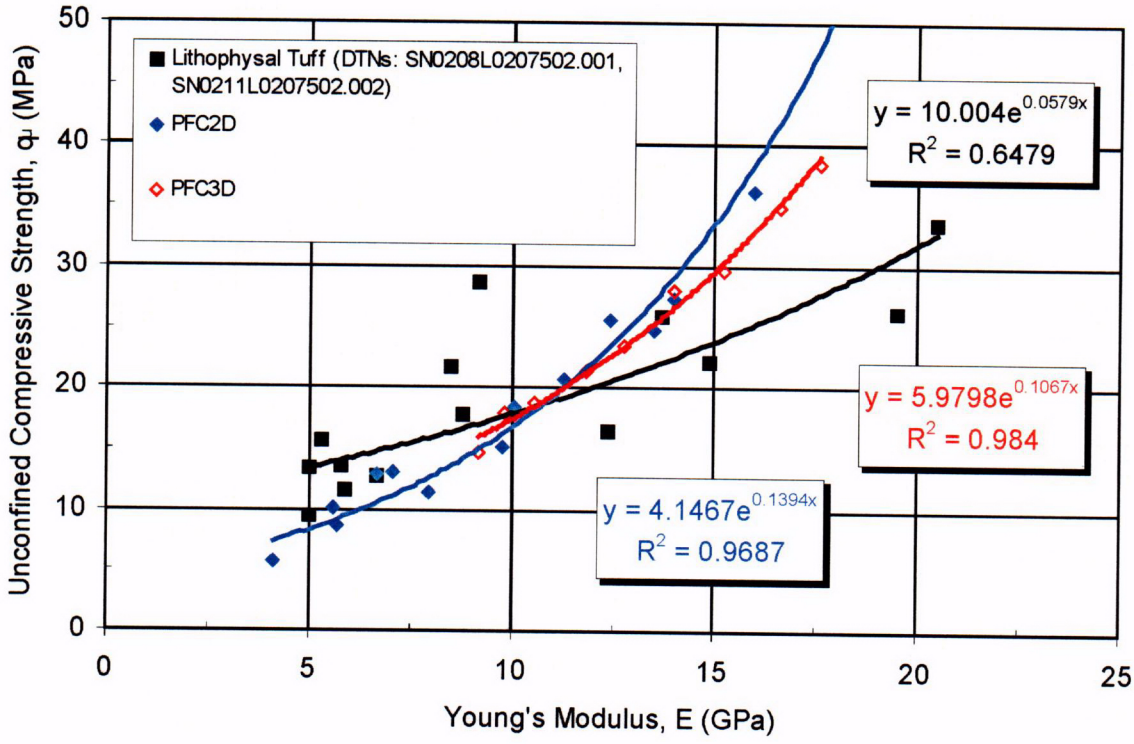

Figure 162. Unconfined Compressive Strength Versus Young's Modulus for Lithophysal Tuff and PFC Materials

7.7 DEVELOPMENT AND VALIDATION OF A DRIFT-SCALE MODELING METHOD FOR LITHOPHYSAL ROCK USING THE UDEC PROGRAM

As was noted in Section 7.1, the PFC program is computationally intensive and, therefore, not particularly practical for use as a modeling tool for drift-scale analyses as required. The method used here is to first calibrate a similar modeling approach based on the UDEC (Section 3.1) discontinuum program to the laboratory data and then validate this approach against (1) observations of failure mechanism in the laboratory, (2) field observations of tunnel response in the ECRB Cross-Drift, and (3) thermally induced fracture development in the Drift Scale Test within the Tptpmn unit. Figure 151 provides a flow chart illustrating the calibration and validation strategy for UDEC. The following section describes the validation of the UDEC model and exploration of its limitations.

7.7.1 Qualification of the UDEC Program

The UDEC program has been qualified as documented in Section 3. The software documentation contained in the UDEC user's manuals (Itasca 2002) provides details of the analytical development of the program and the mechanical basis for the material constitutive models that it uses. Extensive documentation (Itasca 2002) is dedicated to verification of the ability of the model to solve analytical solutions that test the various aspects of the model (e.g., mechanical, thermal, porous media flow, dynamics).

7.7.2 Justification for a Two-Dimensional Isotropic Model of the Lithophysal Rock

As was discussed in Section 7.3, the lithophysal units, particularly lower lithophysal zone (Tptpll), are characterized by the presence of more-or-less uniformly distributed voids (lithophysae) of varying size (from centimeter size to over 1 m in diameter). The lithophysae account for up to about 30 percent of the rock mass. Additionally, in the Tptpll, intense, short trace length interlithophysae fracturing exists. Average joint spacing is on the order of cm to dm, creating block dimensions on the order of the fracture spacings, or cm to dm in dimension.

Under such conditions, representation of lithophysal rock units, in the models of drift stability, as a homogeneous, isotropic rock mass is appropriate. The size of the internal structure and spacing is much smaller than the drift size (i.e., 5.5-m diameter). There is no preferred direction in the orientation that would justify introduction of anisotropy. Heterogeneity was considered on the scale of the repository. The analysis was conducted using different properties of the rock mass to investigate the effect of varying quality of rock mass on drift stability. However, properties inside each model were considered homogeneous. Under such conditions, when there is no internal structure in the model, and properties are isotropic and homogeneous, the drift stability analysis was conducted using a two-dimensional model in the plane perpendicular to the drift axis. The model results of rockfall prediction (in a cross-section characterized by particular rock mass properties) are then used for estimating overall rockfall in the entire repository based on estimated distribution of different rock mass qualities throughout the repository.

7.7.3 Rock Mass Properties for Model Calibration

The rock mass properties for lithophysal rock mass were determined based on:

- Laboratory testing on 10.5-in diameter cores of Tptpll from Busted Butte
- Laboratory testing on 11.5-in diameter cores of Tptpll and Tptpul from ESF main loop and ECRB Cross-Drift
- Three in situ slot tests
- PFC extrapolations of mechanical response under triaxial stress conditions.

The division of rock mass properties into six categories based on the lithophysal porosity and size effect was discussed in Section 7.4.2 and given in Table 45.

7.7.4 Model Calibration

The two-dimensional distinct element code, UDEC (Section 3.1), is used here for drift stability analysis. The rock mass is represented as an assembly of polygonal, elastic blocks (Figure 163) that are bonded together across their boundaries to form a coherent solid. The goal is to provide a rock mass in which the overall mechanical behavior of the mass is consistent with the material model developed for the lithophysal rock, yet allow internal fracturing to form and blocks to loosen and detach as the evolving stress state dictates. In other words, the fractures are "invisible" to the model until yielding begins.

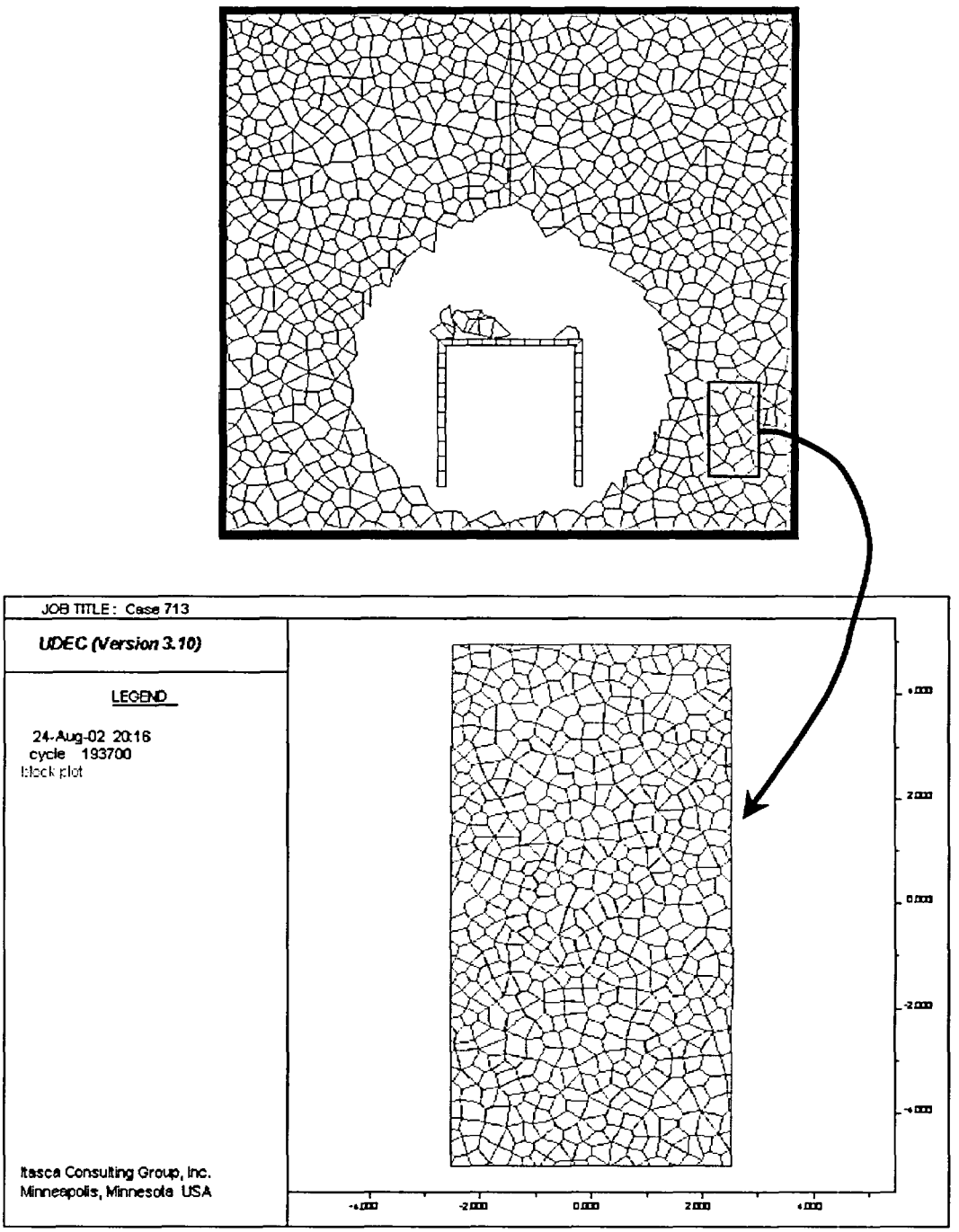

NOTES: Blocks are bonded at their contacts with a cohesion and tensile strength. When these break, the contacts become purely frictional. Specimen is "sampled" from equivalent rock mass representing the Tptpll.

Figure 163. UDEC Lithophysal Rock Specimen Composed of Many Irregular Blocks with Roughly Equi-Dimensional Side Lengths

Since the block boundaries can fail in tension and shear, they act as "potential fracture" locations should the stresses dictate that fracture is possible. It is important that the block assemblage contain blocks that are sufficiently small such that the model does not dictate where and how fractures can form and propagate. The entire tunnel domain is discretized into small blocks (using Voronoi tessellations, see Itasca 2002) that are roughly consistent with the maximum block size expected from core fracture spacings. The potential fractures between blocks are considered to behave mechanically according to a linearly elastic-perfectly plastic model. The elastic behavior of potential fractures is controlled by constant normal and shear stiffness, and are consistent with the Young's modulus of the intact rock blocks. The possible failure modes of the rock mass are controlled by the strength of the fractures. The fractures can sustain a finite tensile stress, whereas a Coulomb slip condition governs the onset of slip, as a function of joint cohesion and friction angle. If a potential fracture fails, either in tension or shear, tensile strength and cohesion are set to zero, whereas the friction angle is set to the residual value. This model allows for the formation of fractures between blocks, separation and instability (under action of gravity) of portions of the rock mass around a drift.

The blocks used in the UDEC model do not represent the actual internal structure of the lithophysal rock mass. They are a tool in the numerical model used to simulate damage and fracturing of the rock mass (i.e., the potential fractures in this model do not correspond to actual features). Therefore, it is not possible to *directly* obtain the potential fracture properties in the UDEC model to results of laboratory or field testing on samples of lithophysal rock. To assure that an assembly of Voronoi blocks behaves as a lithophysal rock mass, it has to be calibrated. Calibration is done by numerical simulation of tests (e.g., unconfined compressive strength tests), which are actually conducted in the laboratory or the field, and for which the test results are available. During the numerical experiment (calibration), the model parameters (i.e., potential fracture properties) are varied until macro-properties of the rock mass important for the drift stability analysis (e.g., Young's modulus and unconfined compressive strength) are matched with measurements from the actual tests. When the calibration is completed it is possible to say that the synthetic material (i.e., the assembly of Voronoi blocks) behaves (on the scale of a drift) equivalently to the lithophysal rock mass. Following calibration, the model can be used to conduct additional simulations under biaxial compression and tension to produce the yield criteria for the material. These yield criteria can be compared to typical empirically derived yield criteria for other rock types as a means of verification of the model.

The following parameters characterize the mechanical behavior of the UDEC Voronoi model:

- The block size scaled to the model size, or a number of blocks in the model.
- Elastic properties of blocks (E^m, ν^m).
- Properties of joints, both elastic (normal stiffness, k_n, and shear stiffness, k_s) and plastic (tensile strength, t^m, cohesion, c^m, and friction, ϕ^m). Note that plastic joint parameters are functions of shear and tensile plastic strains. In the simulations presented in this report, it is assumed that cohesion and tensile strength soften to zero at the onset of yield.

The micro properties are illustrated in Figure 164.

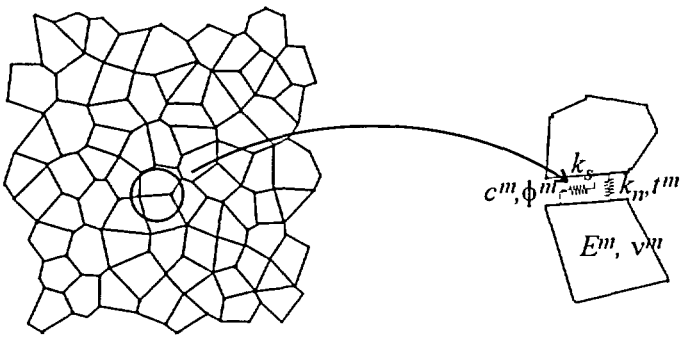

Figure 164. Micro Properties of the UDEC Voronoi Model

Because of the geometrical complexity of the model, a direct functional correlation between micro- and macro-properties (model response on a large scale) does not exist. Therefore, to match model macro-behavior, it is necessary to calibrate the model. During the calibration, which is done during simulation of simple uniaxial and biaxial experiments, the micro-properties are adjusted until the desired macro-behavior is matched. The calibration uses a trial-and-error approach, but some understanding of the model mechanics and previous experience can expedite convergence of the iterative process.

Elastic and strength properties can be decoupled during the iteration process (i.e., model deformability and strength can be calibrated separately). It is common to calibrate model elastic parameters first. Clearly, calibration of the elastic properties is a problem with a non-unique solution. The two elastic macro-properties (E and ν) are functions of block size and four micro properties (k_n, k_s, E^m, and ν^m). The block size is determined based on observed fracture spacing and the condition that the ratio between the drift radius and the block size is sufficiently large (>15). The Poisson's ratio of the blocks is selected to be equal to the macro Poisson's ratio, such that $\nu^m = \nu$. The additional requirement needed to match the macro Poisson's ratio is that the ratio between normal and shear joint stiffnesses is larger than 1. Simulations confirm that a Poisson's ratio of 0.2 is matched when $k_n / k_s \approx 2$. It is reasonable that the contribution of joints to model deformability is larger than the contribution of blocks, but it is desirable, from the perspective of convergence of the numerical model, that stiffnesses of blocks and joints are of the same order of magnitude. Therefore, based on guidance in the UDEC User's Manual (Itasca 2002, Manuals/UDEC/User's Guide/Section 3: Problem Solving, Section 3.2.3), it was selected that

$$5 < \frac{K^m + \frac{4}{3}G^m}{b\,k_n} < 10 \qquad \text{(Eq. 16)}$$

where b is the average block size, and K^m and G^m are the bulk and shear moduli of the blocks, respectively. With these considerations, there is a single independent elastic micro-parameter (e.g., k_n). The proper macro deformability of the model is than matched by rescaling of the elastic micro-properties (k_n, k_s, K^m, and G^m).

Calibration of strength micro properties involves matching macro failure envelope and post-peak behavior by adjusting strength micro-properties. Note that model plastic deformation appears to

be a function of the size and shape of blocks. The failure envelope, which, in general, is a surface in the principal stress space, reduces to a line if it is considered that the failure envelope is not a function of the intermediate principal stress. Test runs have proven that the micro friction angle, which is initially equal to 35° and softens in a brittle fashion to 15°, results in the desired post-peak behavior and strength increase as a function of confinement. In order to match the observed mode of failure of non-lithophysal tuff under unconfined loading conditions (i.e., axial splitting), the micro tensile strength is assigned to be less than 50 percent of the micro cohesion. After these relations are established, the proper peak strength is matched by rescaling micro cohesion and tensile strength.

Stress-strain curves obtained from the numerical experiment for different conditions of confinement (unconfined, 1-MPa confinement, and 3-MPa confinement) and a sense of loading (tension and compression) are shown in Figure 165. The mode of failure is also illustrated for each case by a plot of displacement vectors at the final state of the model. The model matches unconfined compressive strength of 10 MPa and Young's modulus of 1.9 GPa for category 1 (Table 45). Laboratory testing data on the post-peak behavior of lithophysal rock is inconclusive. However, the model exhibits qualitatively reasonable post-peak behavior. The response for low confinement is brittle (see unconfined compressive strength curve in Figure 165). As confinement increases the response becomes more ductile, almost perfectly plastic for 3-MPa confinements (Figure 165). The mode of sample failure in the case of unconfined compressive strength is axial splitting, similarly to observations from laboratory experiments. The mode of failure for confined cases becomes more of the "shear band" type.

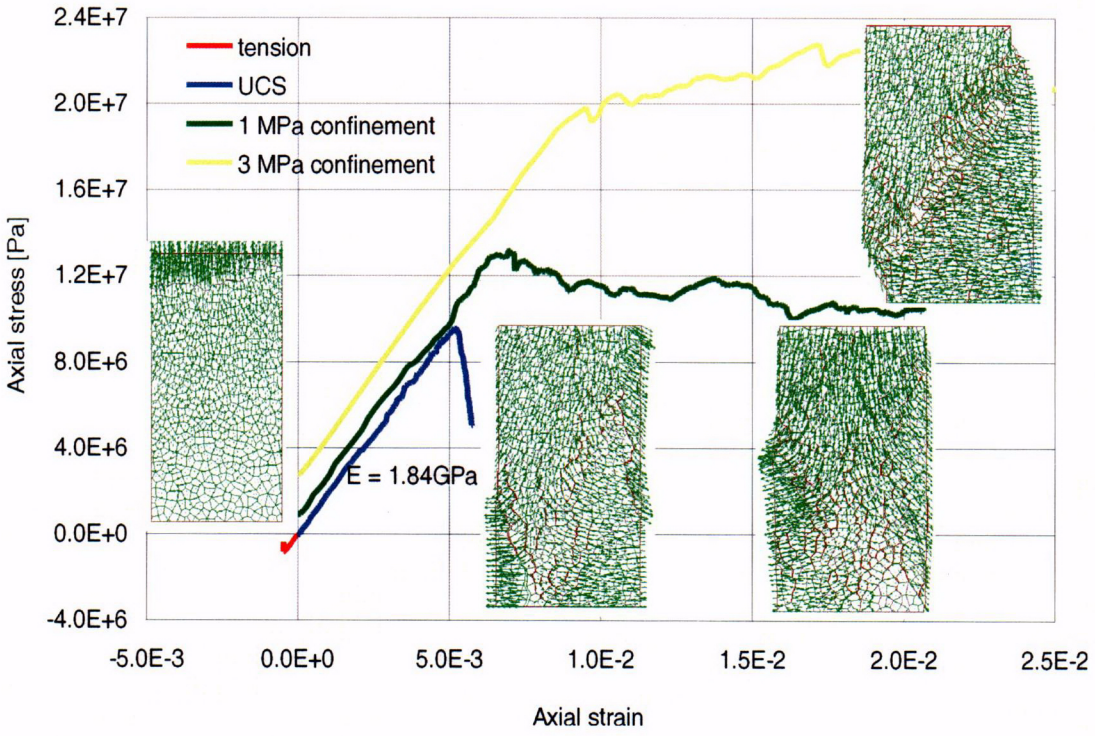

Figure 165. Numerical Experiment, Category 1: Stress-Strain Curves and Modes of Failure for Different Confinements and Loading Conditions

C75

The failure envelope in the principal stress space, constructed based on numerical tests at different confinement levels, is shown in Figure 166. The failure envelope is curvilinear, as expected for a rock mass (similar to Hoek-Brown failure criterion). The initial friction angle (in the range of confining stress, σ_3, between 0 and 1 MPa) is 33°, but it decreases for larger confinement. The ratio between uniaxial compressive and tensile strengths is larger than 10.

The volumetric deformation of the model during the experiments is illustrated in Figure 167, which shows curves of volumetric strain versus axial strain. In general, these curves are bilinear. Initially, while the sample behaves elastically, its volume reduces due to the Poisson's effect. The initial slope of the curves is a function of the Poisson's ratio. Thus, the Poisson's ratio, ν, of the synthetic material can be calculated from the initial slope of the curve, s_e, according to the following formula derived from elasticity theory:

$$\nu = \frac{1 - s_e}{2 - s_e} \qquad \text{(Eq. 17)}$$

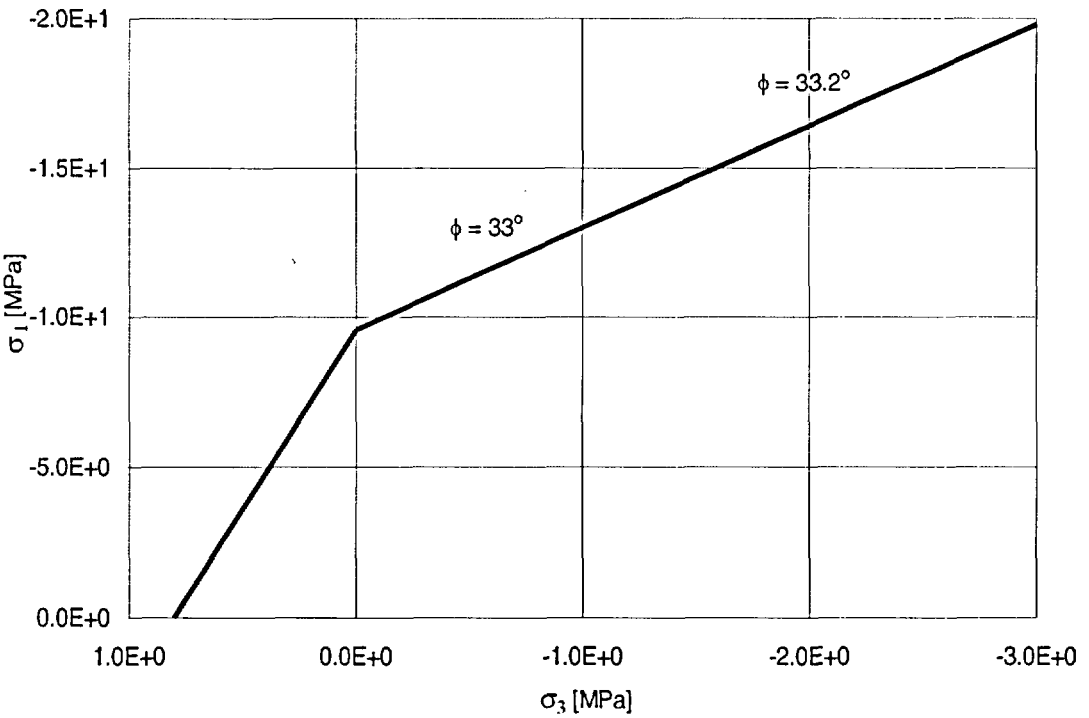

Figure 166. Numerical Experiment, Category 1: Failure Envelope

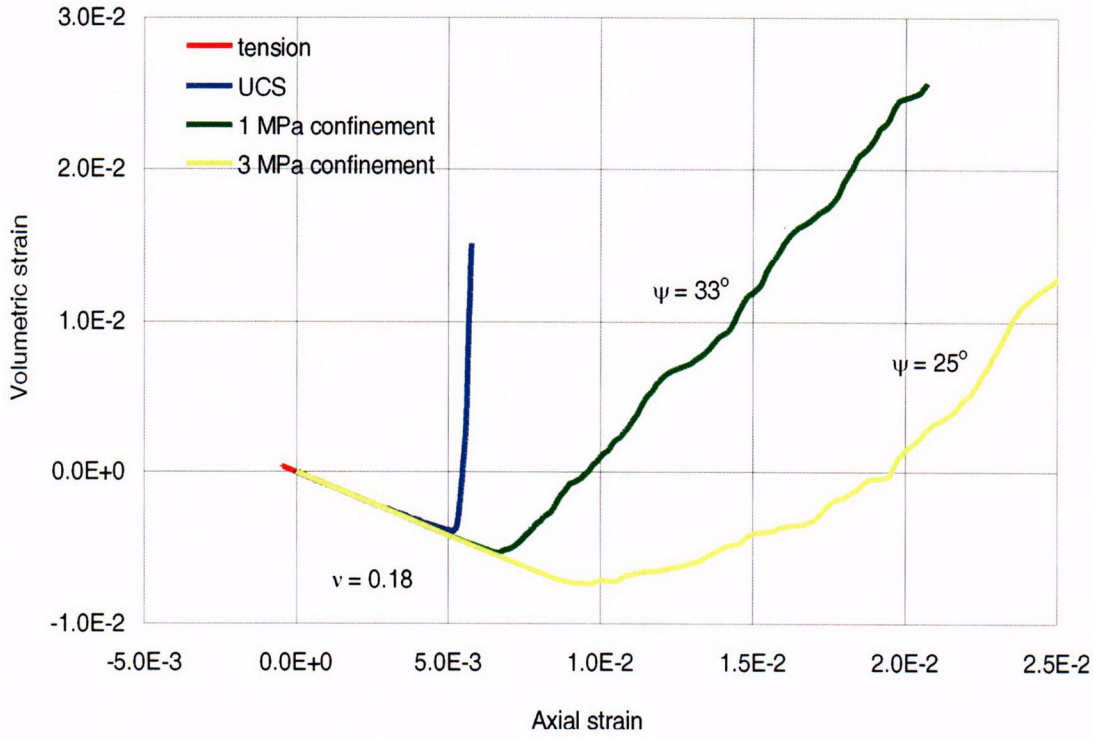

Figure 167. Numerical Experiment, Category 1: Volumetric Strain Versus Axial Strain for Different Confinements and Loading Conditions

As the material yields and starts plastic deformation, it usually dilates (increases volume). Consequently the curves in Figure 167 change the slope. Initially negative slopes, indicating contraction, become positive, indicating dilation. The slope of the curves during plastic deformation is a function of the dilation angle, which is the parameter used to characterize plastic volumetric deformation. The dilation angle, ψ, of the synthetic material can be calculated from the post-peak slope of the curve, s_p, according to the following formula, which was derived from Mohr-Coulomb plastic flow equations in *Itasca Software–Cutting Edge Tools for Computational Mechanics* (Itasca 2002):

$$\psi = \arcsin\left(\frac{s_p}{s_p + 2}\right) \qquad \text{(Eq. 18)}$$

The synthetic material clearly exhibits a very large dilation angle for unconfined compressive strength. Such behavior is expected because micro damage of the material during unconfined compressive strength testing is predominantly tensile fracturing, which results in extremely large dilation.

7.7.5 Validation Strategy

Once calibrated, the UDEC model and properties require validation against field observations and testing. The model is also validated against laboratory failure mechanisms and drift scale response by:

- Comparison of lithophysal sample failure mechanisms in the laboratory
- Comparison of the prediction of drift scale fracturing in the Tptpll at ECRB Cross-Drift depth to observations of tunnel sidewall fracturing in the ECRB Cross-Drift
- Comparison of roof spalling in the Drift Scale Heater Test in the Tptpmn during thermal overdrive experiments to UDEC model predictions
- Comparison of several different numerical modeling techniques to UDEC for a field simulation of steel tube-reinforced tunnel to dynamic loading from a blast.

Additionally, the capabilities of the UDEC program for representing dynamic response of jointed or fractured media is demonstrated by code-to-code comparisons conducted through past dynamic tunnel stability analysis for the Defense Nuclear Agency.

7.7.5.1 Validation Exercise 1 - Comparison of Predicted Failure Modes to Laboratory Observations

The UDEC "potential fracture" model is formulated to allow fractures to form as the stresses dictate. An initial and simple validation is to compare the predictions of the model to observations and common knowledge from laboratory testing. In uniaxial compression, with 2:1 length-to-diameter specimens, the failure mode is typically in the form of axial splitting, or coalescence of axially oriented fractures observable on the surface of the sample. Figure 168 presents a typical UDEC plot of predicted fracturing (red tensile cracks) that form axial to the sample axis. The block structure of the sample was previously shown in Figure 163, but is not shown in Figure 168 so that the formed cracks are clearly seen. The typical laboratory failure response is shown in the associated photograph of a large core sample from the Tptpul after testing. The axial fractures are clearly visible in this photo. The UDEC model further is able to produce typical tensile fracture orientation from a simulated direct tension test (Figure 169). The model will seek out a unique fracture path composed of coalescing "potential fractures" to form a distinct separation plane.

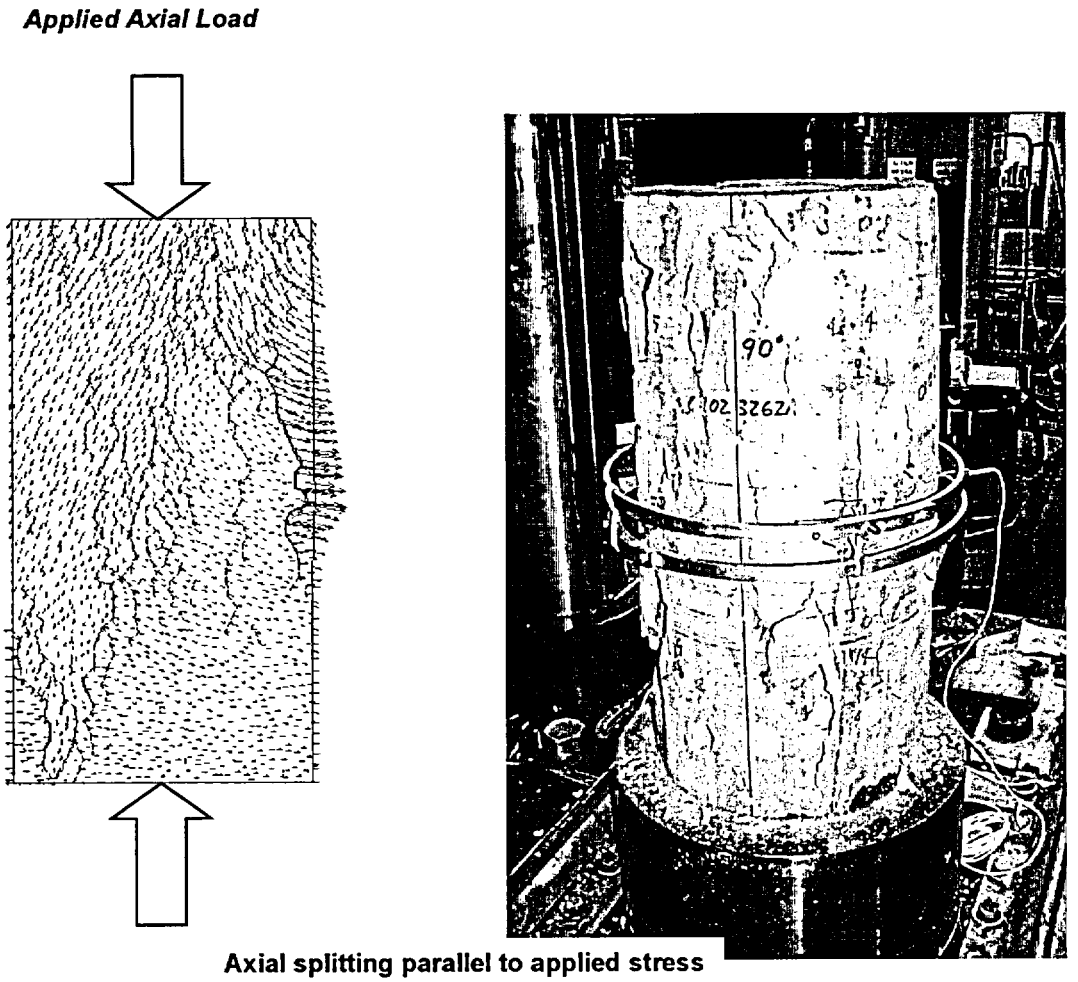

NOTES: The model predicts axial splitting when no confinement is applied as seen by the red tensile block boundary breakages (fractures) formed and by the velocity vectors that show the sidewall spalling. Core photo shows similar axial splitting phenomena.

Figure 168. UDEC Discontinuum Model of Failure of Lithophysal Tuff Specimen Under Uniaxial Compression

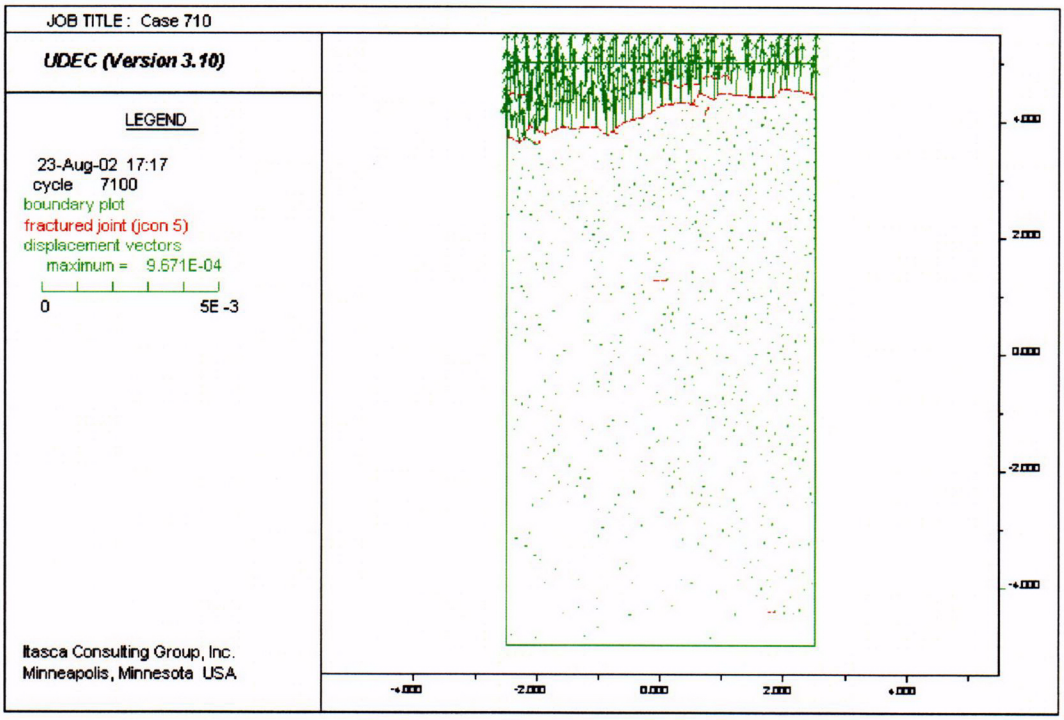

NOTE: A distinct tensile fracture formed from coalescence of individual breakages.

Figure 169. Predicted Failure Mode of UDEC Sample in Direct Tension Test

7.7.5.2 Validation Exercise 2 - Comparison of Model Predictions to Observations in the ECRB Cross-Drift

The proposed modeling approach was verified by comparison of predicted in situ stress-induced damage to the minor damage observed in sidewalls of ESF main loop and ECRB Cross-Drift in the lowest quality Tptpll. Additionally, no sidewall damage is observed in drifts in higher quality Tptpul at shallower depth. Tunnels in all rock units are stable after excavation, regardless of depth or rock quality. However, some damage, in the form of wall parallel fractures (opening of existing fracture fabric) at the springline (the point of highest shearing stress), can be observed in the sidewalls of the tunnels at greater depth in the Tptpll. Figure 170 shows formation/opening of wall-parallel fractures observed in 12-in. diameter boreholes drilled for geomechanical sampling in the sidewalls of the ESF main loop and ECRB Cross-Drift at the tunnel springline. The wall-parallel fractures are typical of stress-induced yield in tunnels. The boreholes drilled in the relatively low quality Tptpll at depths of 300 to 350 m show sidewall fracturing to depths of approximately 0.5 to 0.6 m. Holes drilled into relatively high quality Tptpul at depths of approximately 200 to 250 m show no fracturing.

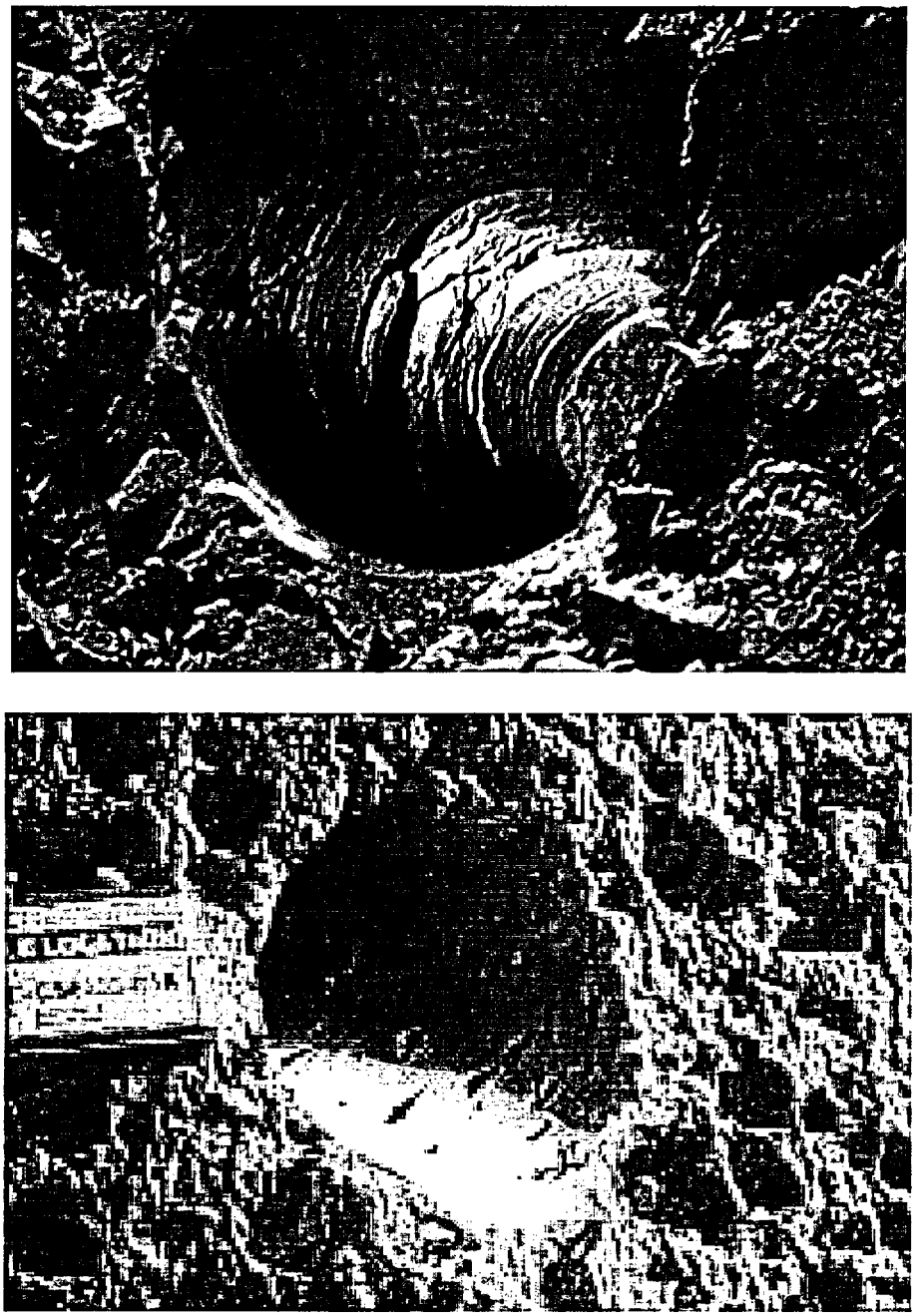

NOTES: Top photo shows sidewall fracturing/opening of preexisting wall-parallel fractures in a 12" diameter horizontal borehole drilled in the springline of the ESF in low quality Tptpll (approximately category 1). Overburden depth is approximately 325 m. Depth of fracturing is approximately 1.5 to 2 ft. The bottom photo shows a horizontal, 12-in diameter borehole drilled in the springline in good quality Tptpul (approximately category 5) in ESF near site of slot test 2 showing no sidewall damage. The depth of overburden is approximately 250 m.

Figure 170. Observed Rock Mass Conditions at the Tunnel Springline in Lithophysal Rock in the ESF

The presence of these fractures and their depth into the drift wall, observed in large hole drilling, is a convenient feature from which an estimate of the rock mass strength properties and

validation of the model can be made. A parametric study of drift stability and rock yield depth was conducted using the UDEC lithophysal model for all 6 strength categories (Table 45) and imposed overburden depths of 250, 300, and 350 m, corresponding to the Tptpll and Tptpul. As seen in Figures 171 and 172, the model reproduces the approximate depth and orientation of drift wall-parallel fractures observed underground for strength category 1. The failure of the rock is contained to the immediate springline due to the stress concentration resulting from the vertical maximum stress (vertical stress in MPa = 0.024×depth (m), horizontal/vertical stress = 0.36 to 0.62). The model results indicate that the rock adjacent to the drift wall yields in a state of uniaxial compression since the minimum stress at or near the drift wall is zero or small since the radial stress component is zero. The depth of fracturing is clearly visible in these models as the zone where stress relaxation has occurred. The models also show that, for the range of potential lithophysal rock properties, there is no drift wall yield at the depth of the Tptpul from strength category 1. Figure 171 compares the model results for strength categories 1 and 6. The extent of rock mass fracturing shown in category 6 indicates that drift wall yielding is likely for category 6 at a depth of 250 m and roof yielding is also predicted for greater depths. These predictions were not observed in the ECRB Cross-Drift. However, the extent of yielding around the opening for category 6 rock is not excessive. For conservatism, rock mass quality category 6 remains the lower bound for the range of rock mass strength.

In conclusion, this validation exercise shows that:

- The model is able to represent the observed wall fracturing at the Tptpll depth and only for a range of rock strengths that agree with laboratory measurements of uniaxial compressive strength (i.e., the observed yield is consistent with laboratory measured values).

- The model shows that reduction of depth to that of the Tptpul results in no yield of the drift wall, and thus no fracturing as observed.

7.7.5.3 Validation Exercise 3 - Comparison of Model to Drift Scale Experiment in the Tptpmn

The Drift Scale Heater Test was conducted in the Tptpmn unit, primarily as a fluid migration experiment (Williams 2001). This test involved driving a 5-m × 5-m drift, 50-m in length completely within the Tptpmn. The drift was heated using simulated electrically heated canisters within the drift itself, as well as horizontally placed borehole heaters in the springline of the tunnel to additionally raise the ambient rock mass temperature (Figure 173). Heating was started in 1997 and lasted for four years until 2001. The experiment is currently in the cool-down phase. After three years of heating (from 1997 to 2000), the heater power was raised to provide a thermal overstressing condition. The rock temperature level was driven to approximately 200°C, or a maximum 180°C temperature rise. Spalling of rock was first observed in late 1999 as small chips of rock on the tunnel invert, however there was no observation of obvious larger rock fragments or bulking in the welded wire fabric. Therefore, it is unknown if these small particles are related to thermal stress effects. In April 2001, obvious loose rock was observed at several locations in the crown of the tunnel, contained behind the wire mesh (Figure 174). At least four zones of loosened rock were observed along the tunnel crown, using the rail mounted remote camera. It is not clear that these are all of the zones of spalling due to the difficulty in

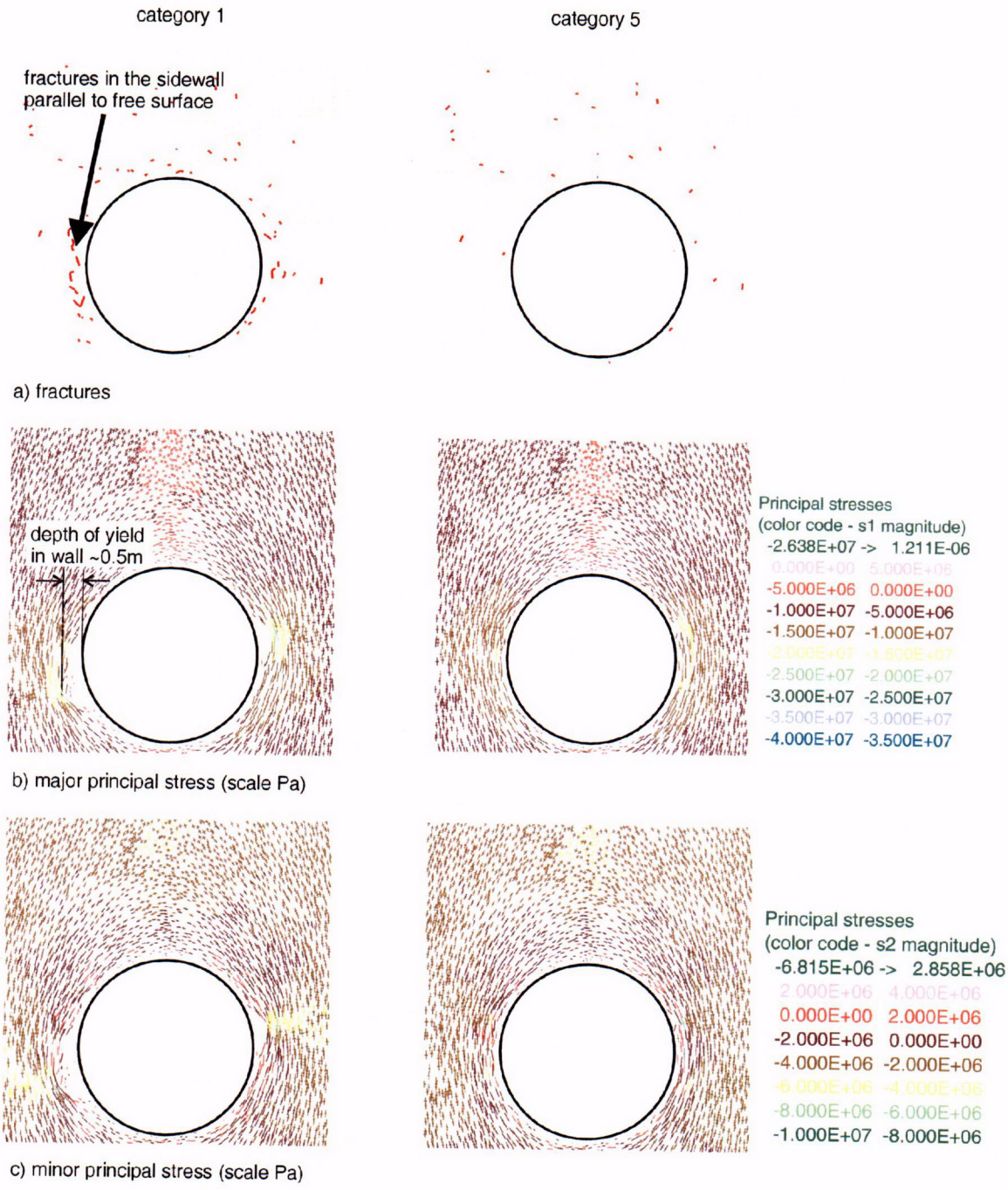

NOTES: Upper figure for category 1 shows predicted fracturing to a depth of approximately 0.5 m in the sidewall of ECRB Cross-Drift. Lower pictures show stress vectors (in Pa) colored by the magnitude of the stress component. Depth of yield for category 1 is limited to about 0.5 m in the immediate springline area. The model for category 5 shows elastic rock mass response (i.e., no yield). Stress vectors in lower figures also show elastic stress distributions with no readjustment due to yielding.

Figure 171. Estimate of Rock Mass Fracturing and Stress State Under In Situ Loading Only, Depth of 300 m, Tptpll, Strength Category 1 (Low-Strength Characteristics) and 5 (High-Strength Characteristics)

C78

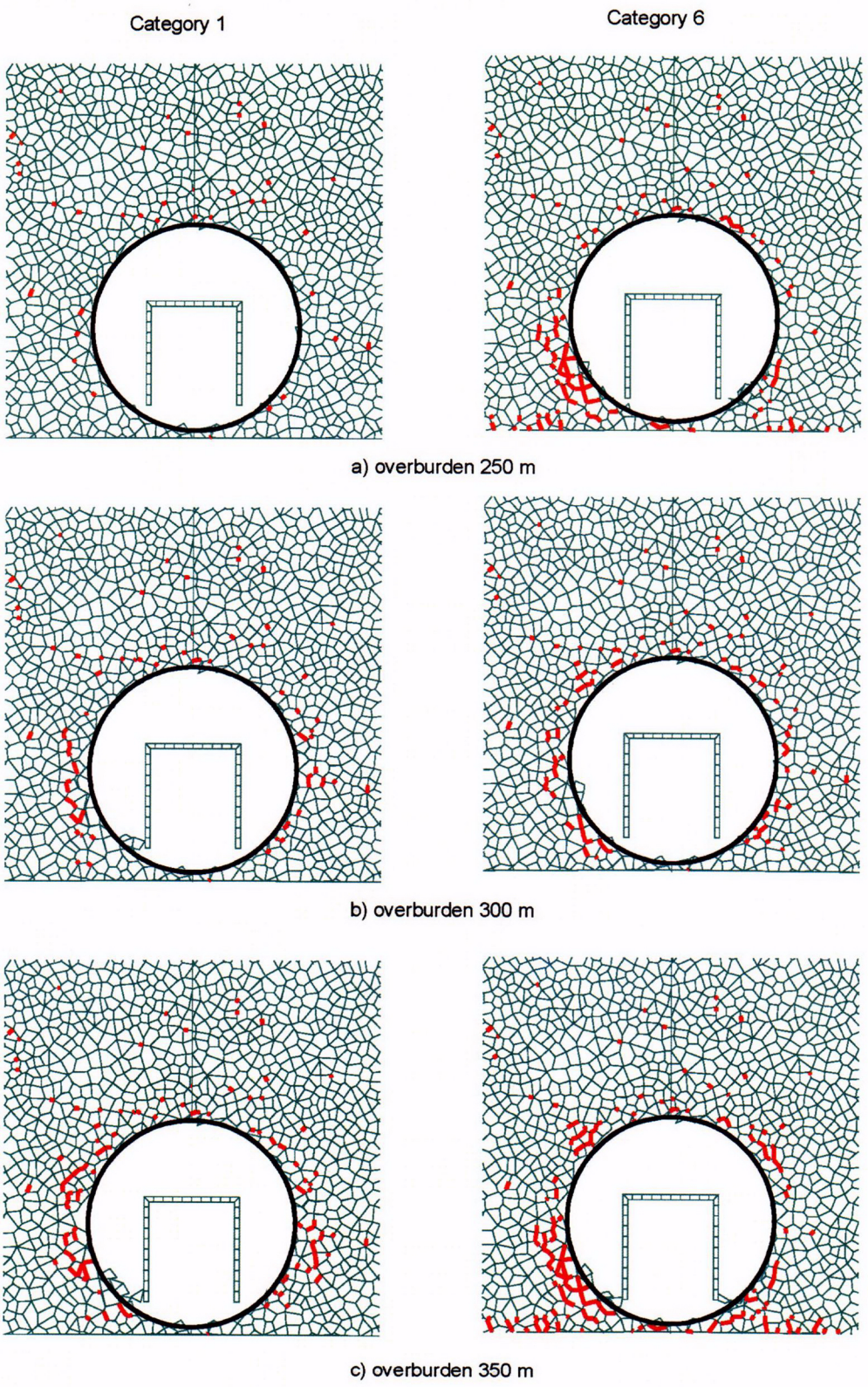

Figure 172. Estimate of Rock Mass Fracturing as a Function of Overburden Between 250 m and 350 m, Tptpll, Strength Categories 1 and 6 (Low-Strength Characteristics)

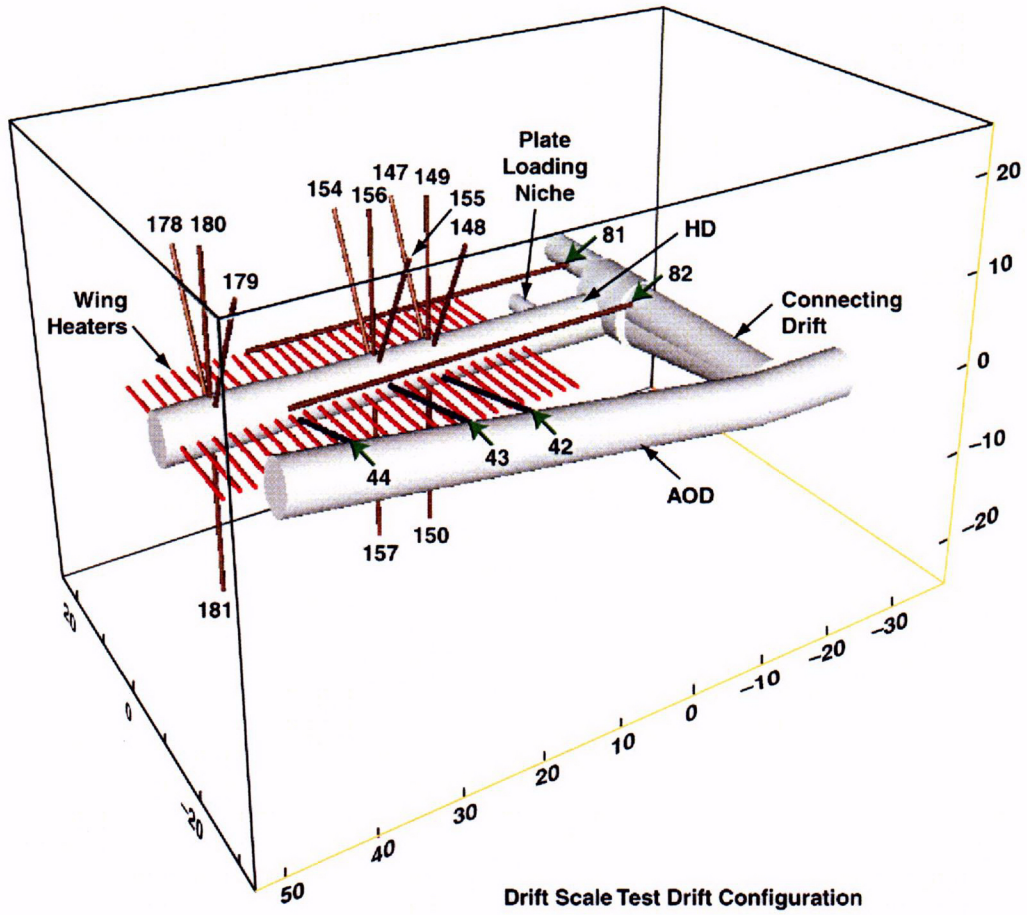

NOTES: HD = Heated Drift; AOD = Access / Observation Drift. Numbered boreholes contain rock mass monitoring instrumentation. Canister heaters are placed in the Heated Drift.

Figure 173. Perspective View of Heated Drift Scale Test Showing Wing Heaters

observation using this camera technique, however, it is clear that they are largely congregated along the tunnel crown. The rock plates held within the welded wire fabric from about 5 to 20 cm. This type of "slabbing" is typical of hard, brittle rock masses subjected to horizontal stresses in the crown that exceed their uniaxial compressive strength.

It is the goal of this validation exercise to demonstrate that the UDEC model with random block subdivision is capable of reproducing thermal fracturing response at the proper approximate temperature and thermally induced stress levels as observed in the Drift Scale Heater Test. The first step in the validation is to calibrate the UDEC "potential" fracture properties against laboratory compression data. A compilation of the results of uniaxial compression strength test data for a range of sample sizes as described by Price (1986) is provided in Attachment V (Figure V-5). The sample sizes vary from 25 mm to approximately 230 mm, resulting in a curve that describes compressive strength as a function of sample size. Since the Drift Scale Heater Test represents in situ sample size, the UDEC model is calibrated to the predicted field scale, represented by a sample size scale of approximately 1-m size, or 70 to 75 MPa, or about 50 percent of the strength of a standard 50-mm diameter sample. This size-strength relationship

compares quite favorably with suggestions for other rock types as used in common practice for rock engineering design purposes. Hoek (2000) suggests that the rock mass strength for a 1-m sample size approaches an approximate value of about 50 to 60 percent of the uniaxial compressive strength of 50-mm cores samples.

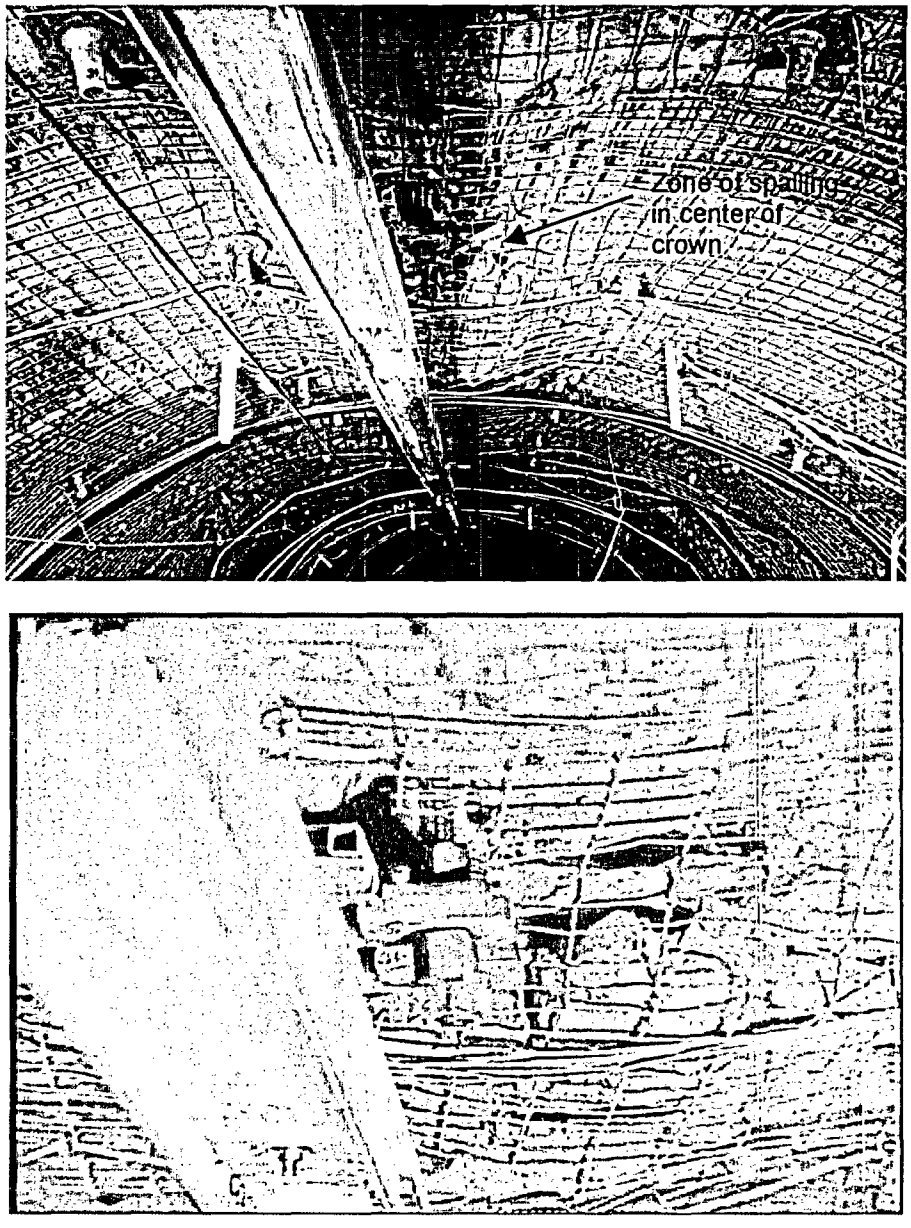

NOTES: Rock spalling is contained by 3-in x 3-in wire mesh and Swellex bolts. Top view shows general spalled region. Bottom view is a close up along the camera rail showing slabbing into small, flat pieces.

Figure 174. Minor Superficial Slabbing in the Center of the Roof Span Observed During Thermal Overstressing of the Heated Drift Scale Test